Brain Struct Funct (2017) 222:2093–2114
DOI 10.1007/s00429-016-1327-5

ORIGINAL ARTICLE

The telencephalon of the Göttingen minipig, cytoarchitecture and cortical surface anatomy

Carsten R. Bjarkam[1,2] · Andreas N. Glud[3] · Dariusz Orlowski[3] · Jens Christian H. Sørensen[3] · Nicola Palomero-Gallagher[4,5]

Received: 19 July 2016 / Accepted: 15 October 2016 / Published online: 24 October 2016

Abstract During the last 20 years pigs have become increasingly popular in large animal translational neuroscience research as an economical and ethical feasible substitute to non-human primates. The anatomy of the pig telencephalon is, however, not well known. We present, accordingly, a detailed description of the surface anatomy and cytoarchitecture of the Göttingen minipig telencephalon based on macrophotos and consecutive high-power microphotographs of 15 µm thick paraffin embedded Nissl-stained coronal sections. In 1-year-old specimens the formalin perfused brain measures approximately 55 × 47 × 36 mm (length, width, height) and weighs around 69 g. The telencephalic part of the Göttingen minipig cerebrum covers a large surface area, which can be divided into a neocortical gyrencephalic part located dorsal to the rhinal fissure, and a ventral subrhinal part dominated by olfactory, amygdaloid, septal, and hippocampal structures. This part of the telencephalon is named the subrhinal lobe, and based on cytoarchitectural and sulcal anatomy, can be discerned from the remaining dorsally located neocortical perirhinal/insular, pericallosal, frontal, parietal, temporal, and occipital lobes. The inner subcortical structure of the minipig telencephalon is dominated by a prominent ventricular system and large basal ganglia, wherein the putamen and the caudate nucleus posterior and dorsally are separated into two entities by the internal capsule, whereas both structures ventrally fuse into a large accumbens nucleus. The presented anatomical data is accompanied by surface renderings and high-power macrophotographs illustrating the telencephalic sulcal pattern, and the localization of the identified lobes and cytoarchitectonic areas. Additionally, 24 representative Nissl-stained telencephalic coronal sections are presented as supplementary material in atlas form on http://www.cense.dk/minipig_atlas/index.html and referred to as S1–S24 throughout the manuscript.

Keywords Brain atlas · Brain mapping · Cortical localization · Cortical areas · *Sus scrofa* · Ungulate

✉ Carsten R. Bjarkam
c.bjarkam@rn.dk

1 Department of Neurosurgery, Aalborg University Hospital, Hobrovej 16-22, 9000 Aalborg, Denmark

2 Institute of Clinical Medicine, Aalborg University, Aalborg, Denmark

3 Center for Experimental Neuroscience (Cense), Institute of Clinical Medicine, University of Aarhus, Aarhus C, Denmark

4 Institute of Neuroscience and Medicine (INM-1), Research Centre Jülich, 52425 Jülich, Germany

5 Department of Psychiatry, Psychotherapy and Psychosomatics, Medical Faculty, RWTH Aachen, Aachen, Germany

Introduction

Large animal neuroscience, e.g., studies on the nervous system in the dog, sheep, pig and primate, offers some advantages compared with small animal neuroscience (Aziz et al. 1992; Chaillou and Tillet 2005; Lind et al. 2007; Bjarkam et al. 2008b; Sauleau et al. 2009; Sørensen et al. 2011; Fast et al. 2013; Dolezalova et al. 2014). The larger animal brain size enables the use of conventional clinical brain imagers and the direct use and testing of neurosurgical procedures and equipment from the human clinic (Lind et al. 2007; Bjarkam et al. 2009, 2010; Fjord-Larsen et al. 2010; Dolezalova et al. 2014). The greater complexity of the large animal brain,

additionally, enables a more direct translation to human brain function in health and disease. Economical, ethical, scientific and practical issues, such as the lack of stereotaxic atlases and devices, proper surgical equipment and housing facilities for normal as well as gene modified large animals, may on the other hand hamper large animal neuroscience (Lind et al. 2007; Dolezalova et al. 2014). Large animal neuroscience should, therefore, either be performed to examine problems specific to large animal species, or to complement promising small animal basic studies by constituting an intermediate research system, bridging small animal central nervous system research to the human (Lind et al. 2007; Bjarkam et al. 2008b; Sauleau et al. 2009; Sørensen et al. 2011; Dolezalova et al. 2014).

During the last 20 years we have used the Göttingen minipig to examine neuromodulatory treatment modalities such as stem cell transplantation, gene therapy and deep brain stimulation directed towards Parkinson disease, obesity, depression and Alzheimer disease (Mikkelsen et al. 1999; Danielsen et al. 2000; Dalmose et al. 2004, 2005; Andersen et al. 2005; Bjarkam et al. 2008b; Fjord-Larsen et al. 2010; Glud et al. 2010, 2011; Ettrup et al. 2012). This has been followed by the development of stereotaxic and surgical approaches needed to manipulate the Göttingen minipig CNS (Bjarkam et al. 2004, 2008a, 2009; Ettrup et al. 2011a, b). The instituted CNS changes have been evaluated in live animals by brain imaging (PET and MR) (Danielsen et al. 1998, 2000; Røhl et al. 2002; Cumming et al. 2003; Andersen et al. 2005), transurethral cystometry (Dalmose et al. 2004, 2005; Jensen et al. 2009), gait analysis (Nielsen et al. 2016), neurological evaluation (Mikkelsen et al. 1999; Nielsen et al. 2016) and by post mortem examination based on histology and stereological analysis (Rosendal et al. 2005; Nielsen et al. 2009, 2016; Glud et al. 2010, 2011).

Several histological atlases covering the subcortical structures of the pig brain are available (Yoshikawa 1968; Szteyn et al. 1980; Salinas-Zeballos et al. 1986; Fèlix et al. 1999) and an MR-based segregation of the pig telencephalon has been provided previously (Watanabe et al. 2001; Saikali et al. 2010). However, a comprehensive and detailed cytoarchitectonic description of the Göttingen minipig telencephalon is lacking, although further studies on cortical activation and neuromodulation would depend highly on such knowledge. The aim of the current paper was, accordingly, to provide a detailed cytoarchitectonic description of the Göttingen minipig telencephalon and its surface anatomy, based on macrophotographs and high-power microphotographs of consecutive Nissl-stained sections.

Materials and methods

Brains were obtained from 22 female Göttingen minipigs (Ellegaard Göttingen Minipigs A/S, Denmark), originally used for experimental surgical studies performed on the thoracic and the vesicourinary system. Thus, only female pigs were used, as urinary catheterization is nearly impossible in male pigs (Ettrup et al. 2011a). Four animals were killed at the age of 4 months, whereas the remaining 18 animals were killed at approximately one year of age (10–14 months). All animals were given an overdose of pentobarbital and then perfused transcardially with 5 l of 4% phosphate buffered paraformaldehyde (pH 7.4) at 4 °C (Ettrup et al. 2011a, b), as approved by the Danish Council for Animal Research Ethics and thus following the "Principles of laboratory animal care" (NIH publication No. 86-23, revised 1985). The brains were removed from the skulls in toto and placed in the fixative for 3–20 days. All brains except one were then divided into 1–1.5 cm thick coronal ($n = 17$), sagittal ($n = 2$) or horizontal ($n = 2$) brain blocks by subsequent HistOmer embedding and sectioning on a HistOtech slicer (Sørensen et al. 2000; Bjarkam et al. 2001). The resulting brain blocks were immersed in 30% sucrose for 7 days and then frozen with gaseous CO_2 before cryostate sectioning into 40 µm (coronal) or 100 µm (horizontal or sagittal) thick sections. The remaining brain from one animal aged 1 year was paraffin embedded in toto and serially sectioned into 15 µm thick coronal sections. Consecutive series were then either Nissl- or myelin-stained. The Nissl-staining was performed for 4 min with 0.1% toluidin blue in citrate buffer (pH 4.0) at room temperature, followed by a rinse in two changes of distilled water and dehydration with three rinses in 99% alcohol, and subsequent xylene infiltration and mounting with Depex. The myelin stain was performed according to our own, previously described, autometallographic development technique (Larsen et al. 2003). Thus, the developer was prepared from a 60 ml gum arabic solution, 10 ml sodium citrate buffer, and 15 ml distilled water with 0.85 g hydroquinone (freshly prepared, dissolved at 40 °C), mixed thoroughly just before use with 15 ml distilled water with 0.12 g silver lactate (dissolved at 40 °C). The sections were covered with the developer for 1 h in a water bath (26 °C) under a light-tight lid. The autometallographic development was stopped by replacing the developer with 5% thiosulphate for 10 min. The sections were then rinsed several times in distilled water before xylene infiltration and mounting with Depex.

All sections were analyzed with a Leica DM5000B microscope with attached digital camera (Leica DFC480). Thus, the cortical cytoarchitecture, cell sizes (estimated diameter of dominant cells) and layering of the prepared

histological sections were identified by direct microscopy and derived qualitative interpretation (by author CRB).

Pictures for atlas figures based on the paraffin embedded Nissl-stained coronal sections (Figs. S1–S24, see http://www.cense.dk/minipig_atlas/index.html), were obtained through a 1.25× objective, while figures demonstrating the cortical cytoarchitecture in detail (Figs. 3, 4, 5, 6, 7) were obtained through a 5× objective. The images were subsequently imported to Adobe Photoshop CC and merged into the final figure automatically. As some figures (S1–S24) are based on more than 80–100 photomerged images, in some instance additional image correction was necessary to obtain a suitable fit. Contrast, light intensity and background of the images were optimized, and large section artifacts and impurities removed for optimal visualization of the telencephalic anatomy. The 24 high-power representative telencephalic coronal sections from the paraffin embedded brain had all major telencephalic structures and cytoarchitectonic fields identified and were subsequently labeled in Adobe Photoshop CC before they were presented as supplementary material in atlas form on http://www.cense.dk/minipig_atlas/index.html, where one may access the images and by use of the scroll function go from whole section visualization to visualization of the distinct cytoachitecture in a given cortical area.

Nomenclature

The nomenclature and abbreviations used will generally follow the principles established by Paxinos and Watson, in their atlas of the rat brain, 6th edition (Paxinos and Watson 2007), although cortical layers are named with roman numerals (I–VI). Naming of lobes and the sulcal pattern are, however, quite species specific, and we have generally tried to follow the previously established nomenclature of the pig brain (Ariëns Kappers et al. 1967), while any digressions here from will be highlighted and discussed in the results and discussion parts of the actual paper.

The identification of major di- and mesencephalic structures will be in accordance with the anatomical studies on the pig thalamus (Solnitzky 1938), the Göttingen minipig subthalamus (Larsen et al. 2004), the Göttingen minipig hypothalamus (Ettrup et al. 2010), and the Göttingen minipig substantia nigra (Nielsen et al. 2009).

Abbreviations

To increase readability, abbreviations are only used to depict anatomical structures on the presented figures, and the used abbreviations will accordingly be explained in the accompanying figure legends. However, both an alphabetic- and a systematic grouped abbreviation list are accessible on http://www.cense.dk/minipig_atlas/index.html.

Results

General considerations

The brains examined in the current study are from animals of either 4 months or approximately one year of age. By examining these brains it became clear that the Göttingen minipig brain continues to grow with increasing age. This finding has previously been substantiated by Jelsing et al. (2006b), who stereologically demonstrated a considerably postnatal increase in cortical neuron number during the first 18–36 months of age. The weight and size of the Göttingen minipig brain will, accordingly, vary with the age of the animal. After a doubling of the weight during the first 3–4 months (time of puberty, Lind et al. 2007) it will increase steadily in size during the forthcoming years (Table 1). The following anatomical and cytoarchitectonic description will, accordingly, be based on microscopic examination of the 1 year old specimens, as the pigs at that time can be considered to be young adults (Göttingen minipigs can be more than 20 years old) and the brain architecture thus fully matured. The formalin perfused brain (Fig. 1) will at this time weigh approximately 69 g (68.5 ± 5.14, mean ± SD, $n = 18$) and have a length from the frontal pole to the caudal end of cerebellum of approximately 55 mm (54.6 ± 2.3), while the width measured from the one temporal extreme to the other is approximately 47 mm (46.5 ± 1.9), and the height from the ventral brain stem to the neocortical vertex is approximately 36 mm (35.8 ± 2.4).

General surface anatomy

The Göttingen minipig brain can, based on surface structures, easily be divided into a cerebrum, a cerebellum, and

Table 1 Data obtained from the Göttingen minipig correlating age with average brain and body weight

	Neonate (1–2 days) ($n = 5$)[a]	4 months ($n = 4$)	12 months ($n = 18$)	18–36 months ($n = 5$)[a]
Brain weight (g)	27.8	58.8	69.0	79.0
Body weight (kg)	0.56	17.0	24.9	37.9

Note that the data from the neonate and 18–36 months age group is taken with permission from the publication of Jelsing et al. (2006b)

[a] Jelsing et al. (2006b)

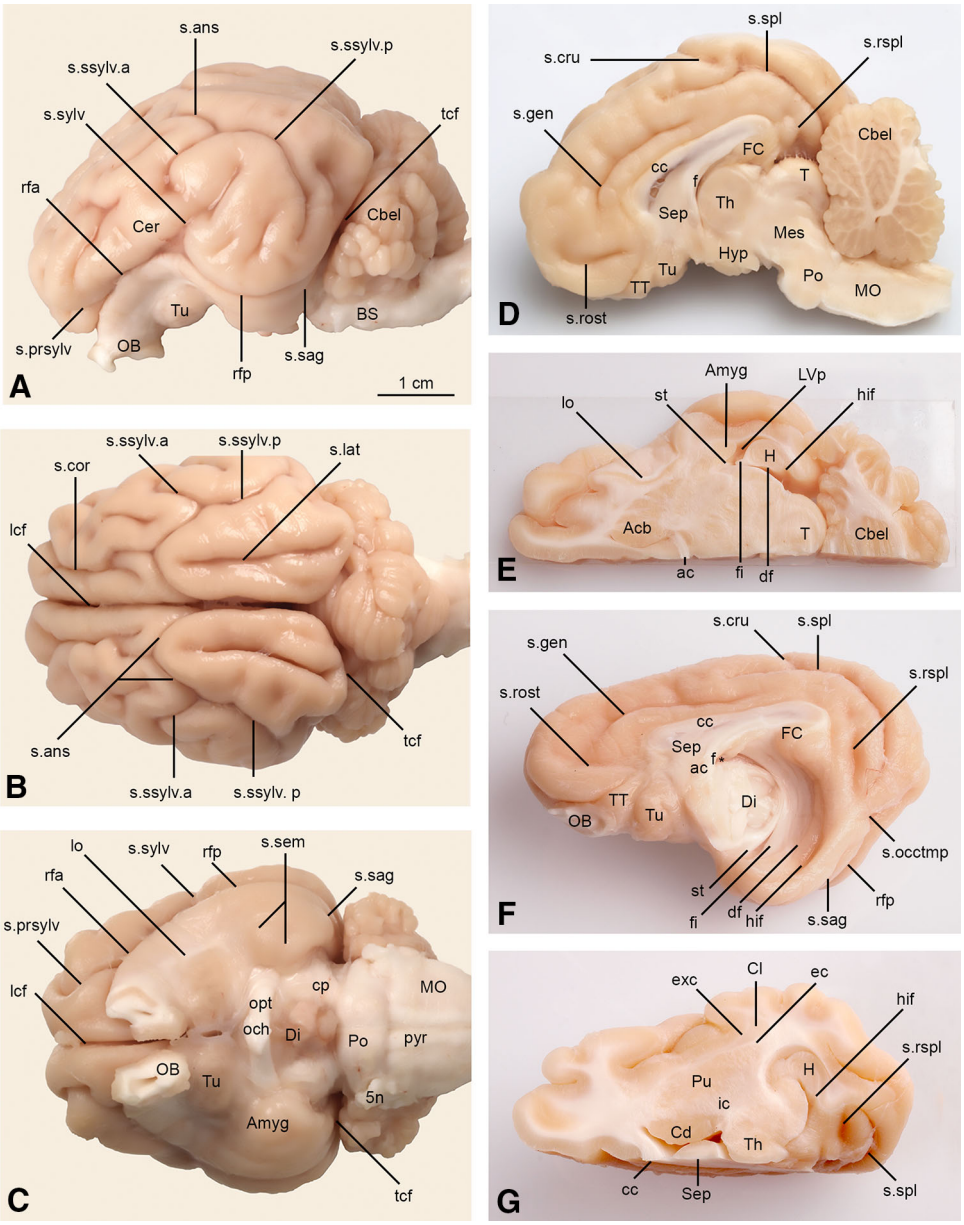

Fig. 1 Macrophotos of the Göttingen minipig brain shown in 150% oversize (see *scale bar* in **a**) depicting its macroscopic anatomy after removal from the skull cavity. Note, that the process of dural opening and brain extraction (Bjarkam et al. 2016), results in tearing of the olfactory bulbs and in absence of the pituitary and the pineal gland. **a** Lateral view, the anterior (rfa) and the posterior (rfp) parts of the rhinal fissure separates the cerebrum into a dorsal gyrencephalic part and a ventral subrhinal part. **b** Dorsal view, the ansate sulcus (s.ans) forms an important landmark. **c** Ventral view, the semiannular sulcus (s.sem) marks the position of the amygdala (Amyg). **d** Midsagittal section, the cruciate sulcus (s.cru) can continue directly in the dorsally located ansate sulcus or originate independently in front of the ansate sulcus, which then will be visible on the mesial side of the brain (compare with Fig. 8). **e** Ventral horizontal section through the anterior commissure (ac). **f** Midsagittal view after removal of the brain stem. **g** Dorsal horizontal section through the genu of the corpus callosum (cc), note the position of the internal (ic), external (ec) and extreme (exc) capsules separating the caudate nucleus (Cd), the putamen (Pu), and the claustrum (Cl). *ac* anterior commissure, *Acb* accumbens nucleus, *Amyg* amygdala, *BS* brain stem, *Cbel* cerebellum, *cc* corpus callosum, *Cd* caudate nucleus, *Cer* cerebrum, *Cl* claustrum, *cp* cerebral peduncle, *df* dentate fissure, *Di* diencephalon, *ec* external capsule, *exc* extreme capsule, *f* fornix, *FC* fasciola cinereum, *fi* fimbria, *H* hippocampus, *hif* hippocampal fissure, *Hyp* hypothalamus, *ic* internal capsule, *lcf* longitudinal cerebral fissure, *lo* lateral olfactory tract, *LVp* lateral ventricle posterior part, *Mes* mesencephalon, *MO* medulla oblongata, *OB* olfactory bulb, *och* optic chiasm, *opt* optic tract, *Po* pons, *Pu* putamen, *pyr* pyramis, *rfa* rhinal fissure anterior part, *rfp* rhinal fissure posterior part, *s.ans* ansate sulcus, *s.cor* coronal sulcus, *s.cru* cruciate sulcus, *Sep* septum, *s.gen* genual sulcus, *s.lat* lateral sulcus, *s.occtmp* primitive occipitotemporal sulcus, *s.prsylv* presylvian sulcus, *s.rost* rostral sulcus, *s.rspl* retrosplenial sulcus, *s.sag* sagittal sulcus, *s.sem* semiannular sulcus, *s.spl* splenial sulcus, *s.ssylv.a* suprasylvian sulcus anterior part, *s.ssylv.p* suprasylvian sulcus posterior part, *s.sylv* sylvian sulcus, *st* stria terminalis, *T* tectum, *tcf* transverse cerebral fissure, *Th* thalamus, *TT* taenia tecta, *Tu* olfactory tubercle, *5n* trigeminal nerve, *asterisk* in **f** marks the interventricular foramen

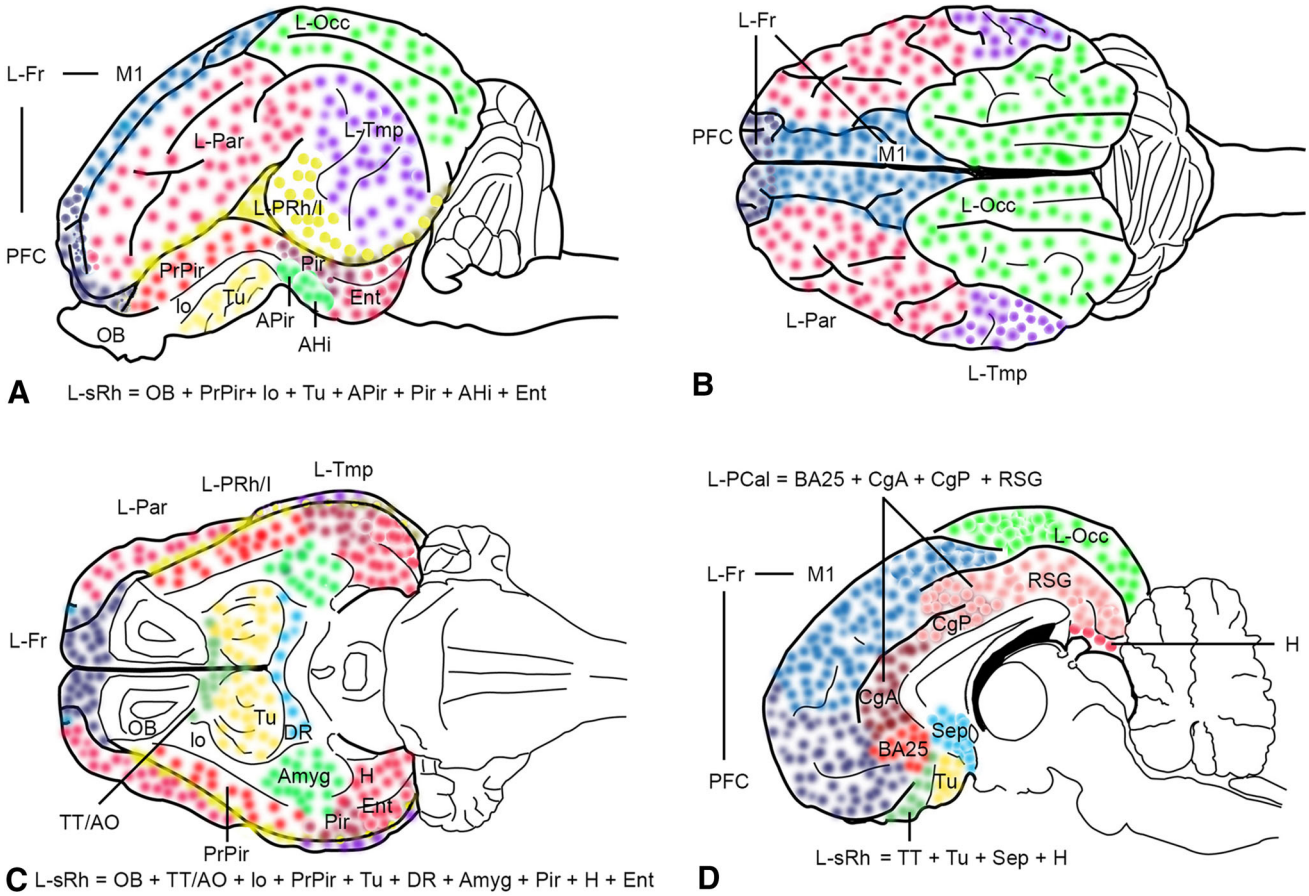

Fig. 2 Schematic drawings corresponding to Fig. 1a–d, respectively, depicting the segregation of the Göttingen minipig telencephalon into lobes and some of their major subareas. **a** Lateral view, note that the visible subareas of the frontal lobe (L-Fr) e.g., the prefrontal cortex (PFC) and the motor cortex (M1) are indicated separately. The visible areas constituting the subrhinal lobe (L-sRh) are likewise indicated and listed schematically. **b** Dorsal view, note that the two subareas of the frontal lobe are indicated separately. **c** Ventral view, the visible subareas of the subrhinal lobe are depicted and listed schematically. **d** Midsagittal view, the visible subareas of the frontal-, pericallosal- and subrhinal lobes are indicated and listed separately. *AHi* amygdalohippocampal transition area, *Amyg* amygdala, *AO* anterior olfactory nucleus, *APir* amygdalopiriform transition area, *BA25* subgenual cortex, *CgA* anterior cingulate cortex, *CgP* posterior cingulate cortex, *DR* diagonal region, *Ent* entorhinal cortex, *H* hippocampus, *L-Fr* frontal lobe, *lo* lateral olfactory tract, *L-Occ* occipital lobe, *L-Par* parietal lobe, *L-PRh/l* perirhinal/insular lobe, *L-sRh* subrhinal lobe, *L-Tmp* temporal lobe, *M1* motor cortex, *OB* olfactory bulb, *PFC* prefrontal cortex, *Pir* piriform cortex, *PrPir* prepiriform cortex, *RSG* retrosplenial granular cortex, *Sep* septum, *Tu* olfactory tubercle, *TT* taenia tecta

a brain stem (Fig. 1a). The brain stem can further be divided into a mesencephalon, a pons and a medulla oblongata by identification of prominent surface structures such as the interpeduncular fossa and the tectum, the pontine prominence, and the pyramids (Fig. 1c, d). The diencephalic part of the cerebrum is only identifiable on surface views from the ventral side (Fig. 1c), where the floor of the hypothalamus can be identified by the location of the optic chiasm, the pituitary stalk (the pituitary gland will normally remain in the pituitary fossa during brain removal) and the mammillary bodies. A midsagittal section (Fig. 1d) will additionally reveal the third ventricle and a prominent thalamic adhesion, while the pineal gland is often separated from the brain during the removal of the meninges, and, therefore, is not present on Fig. 1. The telencephalic part of the cerebrum covers a large surface area which can be divided into a neocortical gyrencephalic part located dorsal to the rhinal fissure and a subrhinal part dominated by olfactory, septal, amygdaloid and hippocampal structures (Figs. 1, 2). The subrhinal part of the telencephalon is named the subrhinal lobe, and is discerned from the remaining dorsally located primarily neocortical perirhinal/insular, pericallosal, frontal, parietal, temporal and occipital lobes based on cytoarchitectural features (Fig. 2; Table 2).

Surface anatomy of the subrhinal lobe

The subrhinal lobe is mainly located frontal and lateral to the hypothalamic floor structures on the ventral side of the

Table 2 Schematic arrangement of data on the "neocortical" suprarhinal lobes obtained by microscopic examination of the paraffin embedded coronal sectioned Göttingen minipig brain presented in Figs. 3c, 5 and 6, and in Figs. S1–S24 of the web based supplementary material

Lobe Cortical area	Granularity	Cortical thickness/ cellular density	Size (μm) of layer V cells	Special features
Frontal (L-Fr)				
Prefrontal (PFC)	Agranular	1.8 mm/low	20–25	Coarse cells. Nearly no difference between layer III and layer V cells
Motor (M1)	Agranular	1.6 mm/low	35–45	Size of layer V cells. Proximal dendrite often visible. Clear distinction to layer III cells ~15–20 μm in size
Parietal (L-Par)				
Somatosensory (dS1)	"Granular"	2 mm/high	15–20	Nearly no size and shape difference between cells in layer II–III–IV
Somatosensory (vS1)	"Granular"	2 mm/medium	15–20	Thicker layer I. Columnar radial arrangement of the more widely spaced cells in layer II–III–IV
Temporal (L-Tmp)				
Temporal (Tmp1)	"Granular"	2.2 mm/medium	15–22	Thicker cortex. More coarse and uneven arranged cells than seen in dS1
Occipital (L-Occ)				
Peristriate (BA18/19)	"Granular"	1.4 mm/high	15–20	Thin cortex. Cellular density decreasing from layer II to layer V. Well developed layer VI
Visual (V1)	"Granular"	2 mm/high	12–18	Thick layer III–IV containing homogeneous small (10–12 μm) pyramids, slightly smaller than the more widely dispersed layer V pyramids
Perirhinal/insular (L-PRh/I)				
Insula (AI)	Agranular	2.5 mm/low	20–25	Thick layer I. Coarse cells. Less clear segregation between layer III–V
Insula (GI)	Dysgranular	2.5 mm/medium	20–25	Increased thickness of layer III which is more clearly separated from the layer V pyramids
Perirhinal (PRh35)	Agranular	1.6 mm/low	20–30	Increasing cell size from layer II to V. Low cellular density in layer III
Perirhinal (PRh36)	"Granular"	2 mm/medium	20–25	Increased number of cells in layer III/IV. Well developed layer VI
Pericallosal (L-PCal)				
Subgenual (BA25)	Agranular	1.2 mm/columnar	15–20	Columnar arrangement of white matter and cells in layer II/III. No distinct difference between layer III and layer V pyramids. Thin layer VI
Cingulate (CgA)	Agranular	1.5 mm/low	20–25	Densely arranged layer II cells. No distinct difference between layer III and layer V pyramids
Cingulate (CgP)	Dysgranular	1.8 mm/medium	20–25	Layer III cells more dispersed and smaller, clear difference to layer V
Retrosplenial (RSG)	Granular	1.7 mm/high	15–20	Real granules (~5 μm) in layer IV
Retrosplenial (RSA)	Agranular	1.4 mm/high	12–18	Few granules. Less well segregated cells in layer II, III. Small-moderately sized pyramids in layer V

Note a real granular layer only is found in the granular retrosplenial cortex, whereas "granular" denote cortical areas with high cellularity and many rows of evenly sized (10–15 μm) pyramids in layer III/IV, that are slightly smaller than the corresponding layer V pyramids

cerebrum (Fig. 1c). Frontally the olfactory bulb forms a large almond shaped structure (Figs. 1a, 2a; Figs. S3–S9). The olfactory bulbs are lowered into a large skull base depression in the anterior cranial fossa (Kyllar et al. 2014). They are here attached to the skull cribrosal plate by the olfactory nerve (fila olfactoria) and they will, therefore, often suffer some degree of tearing during removal from the skull base (Bjarkam et al. 2016), giving them a fringed appearance ventrally (Fig. 1a, c). The olfactory bulb continues posterior and mesial via the medial extension of the anterior olfactory nucleus into a small triangular shaped area, which constitutes the taenia tecta (Figs. 1d, f, 2c, d; Figs. S5–S9), while it laterally, via the lateral extension of the anterior olfactory nucleus, continues into the lateral

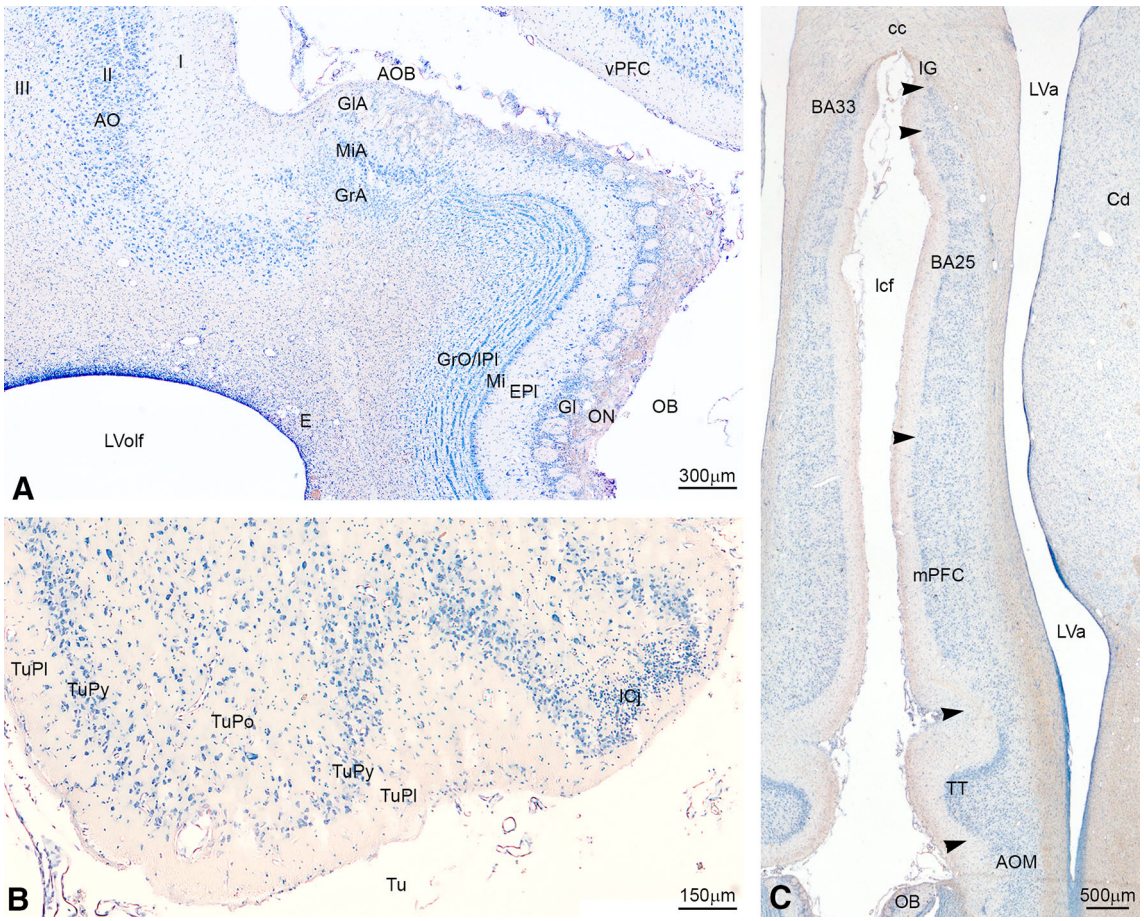

Fig. 3 **a** High-power microphotograph from the ventral part of a Nissl-stained coronal section (Fig. S4) depicting part of the olfactory bulb (OB) incl. the accessory bulb (AOB) and the anterior olfactory nucleus (AO). **b** High-power microphotograph from the ventral part of a Nissl-stained coronal section (Fig. S12) depicting part of the olfactory tubercle (Tu). **c** Microphotograph from the ventral part of a Nissl-stained coronal section (Fig. S7) depicting the subgenual region. *Arrowheads* indicate the transition between the different cortical subareas. *AO* anterior olfactory nucleus, *AOB* accessory olfactory bulb, *AOM* anterior olfactory nucleus medial part, *BA25* subgenual cortex, *BA33* Brodmann area 33 homolog cortex, *cc* corpus callosum, *Cd* caudate nucleus, *E* ependyma and subependymal layer, *EPl* external plexiform layer of the olfactory bulb, *Gl* glomerular layer of the olfactory bulb, *GlA* glomerular layer of the accessory olfactory bulb, *GrA* granule cell layer of the accessory bulb, *GrO* granule cell layer of the olfactory bulb, *Icj* island of Calleja, *IG* indusium griseum, *lcf* longitudinal cerebral fissure, *lPl* internal plexiform layer of the olfactory bulb, *LVa* lateral ventricle anterior part, *LVolf* lateral ventricle olfactory part, *Mi* mitral cell layer of the olfactory bulb, *MiA* mitral cell layer of the accessory bulb, *mPFC* prefrontal cortex medial part, *OB* olfactory bulb, *ON* olfactory nerve layer, *TT* taenia tecta, *Tu* olfactory tubercle, *TuPl* plexiform layer of the olfactory tubercle, *TuPo* polymorph layer of the olfactory tubercle, *TuPy* pyramidal layer of the olfactory tubercle, *vPFC* prefrontal cortex ventral part

olfactory tract and the prepiriform cortex (Figs. 1a, c, 2a, c; Figs. S5–S9). Posterior to the olfactory bulb the olfactory tubercle forms a large ovoid mass of shrunken gray substance constituting a main part of the telencephalic floor (Figs. 1a, c, d, f, 2a, c, d; Figs. S9–S13). The olfactory tubercle is laterally separated from the prepiriform cortex by the lateral olfactory tract (Figs. 1a, d; Figs. S8–S11), while posteriorly it is separated from the diencephalic optic chiasm and optic tract by the slender diagonal region (Figs. 1c, d, 2c, d; Fig. S13). The remaining posterior part of the telencephalic floor is located lateral to the diencephalic floor structures and constitutes medially the amygdaloid prominence, formed by the periamygdaloid cortex overlying the deeper located nuclei of the amygdala (Figs. 1c, 2c). The amygdaloid prominence is posteriorly separated from the temporal pole of the hippocampal formation by a slight indentation in the floor of the telencephalon, named the semiannular sulcus (Fig. 1c). The semiannular sulcus separates likewise the periamygdaloid cortex laterally from the posterior continuum of the prepiriform cortex which now is named the piriform cortex, to separate it from the prepiriform cortex, located lateral to the olfactory bulb and olfactory tubercle (Fig. 1c; Figs. S14–S18). The hippocampal formation (see also Fig. 4e), which encompasses the hippocampus, the dentate gyrus, the subiculum, the presubiculum, the parasubiculum, and the entorhinal cortex, constitutes the most posterior part of the subrhinal lobe located between the corpus

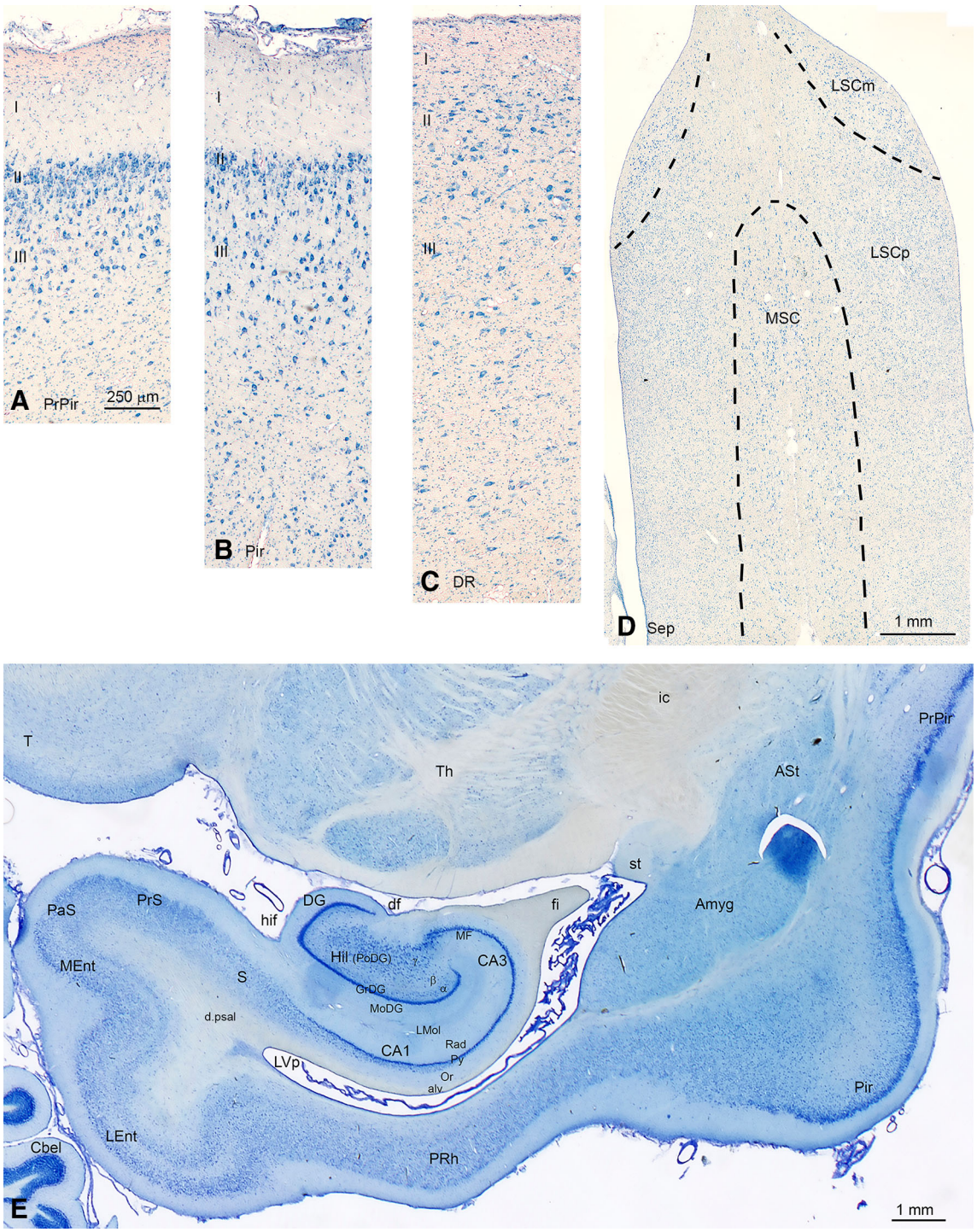

callosum and the retrosplenial cortex mesially (Fig. 1e, f) and the rhinal fissure laterally (Figs. 1b, c, 2a, c; Fig. S15–S24). Posterior and parallel to the rhinal fissure, the sagittal sulcus divides the entorhinal cortex into a medial entorhinal area and a lateral entorhinal area (Figs. 1c, e, f, 4e).

On a midsagittal section revealing the mesial surface of the hemisphere, after removal of the brainstem, one may appreciate the mesial curvilinear structures formed by the fimbria and the hippocampal CA3 area, the dentate gyrus, and the presubiculum/subiculum, separated, respectively, by the dentate fissure and the hippocampal fissure (Fig. 1f, see also Fig. 4e). The fimbria and the septal part of the hippocampal formation run septally below the posterior part of the corpus callosum, while they anteriorly dispatch the fornix. The fornix approaches the anterior commissure located in the septal area, and will here split up into a pre-

◀**Fig. 4** **a** Microphotograph from the ventrolateral part of a Nissl-stained coronal section (Fig. S12) depicting the three-layered prepiriform cortex (PrPir). **b** Microphotograph from the ventrolateral part of a Nissl-stained coronal section (Fig. S17) depicting the three-layered piriform cortex (Pir), which has a more prominent layer III compared to the prepyriform cortex. **c** Microphotograph from the ventral part of a Nissl-stained coronal section (Fig. S13) depicting the three-layered diagonal region (DR). Note the thin layer I and the wide but very diffuse layer III. **d** Microphotograph from the ventromedial part of a Nissl-stained coronal section (Fig. S11) depicting the septum (Sep). The magnocellular medial- and lateral septal complexes have tentatively been segregated from the high-density parvocellular lateral septal complex. **e** Low-power microphotograph of a Nissl-stained horizontal section through the posterior part of the subrhinal lobe depicting the hippocampal formation and its relation to the amygdala and the posterior part of the lateral ventricle. α the outer hilar cell layer, *alv* alveus, *Amyg* amygdala, *ASt* amygdalostriatal transition area, β the inner hilar plexiform layer, *Cbel* cerebellum, *df* dentate fissure, *DG* dentate gyrus, *d.psal* dorsal psalterium, *DR* diagonal region, *fi* fimbria, γ the inner hilar cell layer, *GrDG* granular layer of the dentate hilus, *hif* hippocampal fissure, *Hil* hilus of the dentate gyrus, *ic* internal capsule, *LEnt* lateral entorhinal cortex, *LMol* lacunosum moleculare layer of the hippocampus, *LSCm* lateral septal complex magnocellular part, *LSCp* lateral septal complex parvocellular part, *LVp* lateral ventricle posterior part, *MEnt* medial entorhinal cortex, *MF* mossy fiber layer, *MoDG* molecular layer of the dentate gyrus, *MSC* medial septal complex, *Or* oriens layer of the hippocampus, *PaS* parasubiculum, *Pir* piriform cortex, *PoDG* polymorph layer (hilus) of the dentate gyrus, *PRh* perirhinal cortex, *PrPir* prepirifom cortex, *PrS* presubiculum, *Py* pyramidal layer of the hippocampus, *Rad* radiatum layer of the hippocampus, *S* subiculum, *Sep* septum, *st* stria terminalis, *T* tectum, *Th* thalamus

and post-commissural part (Fig. 1d, f). The corpus callosum continues frontally until it bends nearly 90° ventrally forming the genu of the corpus callosum to continue in its rostral part (Fig. 1d). The septal area is accordingly placed between the rostrum of the corpus callosum and the post-commissural fornix, while it ventrally, without a sharp demarcation, continues into the subgenual area, the olfactory tubercle, and the diagonal region, successively (Figs. 1d, f, 2d).

Surface anatomy of the telencephalon located dorsal to the rhinal fissure

The telencephalon located dorsal to the rhinal fissure has several primary sulci and fissures, which may be used to divide this primarily neocortical part into distinct lobes. In the midline the longitudinal cerebral fissure divides the telencephalon into two hemispheres (Fig. 1b). On the mesial side of the hemisphere the cruciate sulcus is depicted just dorsally to the anterior part of the splenial sulcus (Figs. 1d, 2d). The cruciate sulcus continues as the ansate sulcus on the dorsolateral surface of the hemisphere (Figs. 1a, b, 2a, b) in anterior and then posterior direction before it reaches the suprasylvian sulcus (Figs. 1a, b, 2a, b). The cruciate and ansate sulci form an important landmark, as they separate the posteriorly located occipital lobe from the anterior located frontal and parietal lobes (Fig. 2a, b). On the dorsal surface of the hemisphere one notices furthermore, separated by the ansate sulcus, two sulci, respectively, named the coronal sulcus and the lateral sulcus, which run parallel to the longitudinal fissure (Fig. 1b). The coronal sulcus separates the frontal lobe from the more laterally located parietal lobe (Fig. 2b), while the lateral sulcus is placed centrally in the occipital lobe. On the lateral side of the hemisphere one sees the departure of the sylvian sulcus from the midsection of the ventrally located rhinal fissure (Fig. 1a). The sylvian sulcus is dorsally surrounded by the suprasylvian sulcus, which posteriorly separates the temporal lobe from the occipital lobe, whereas the anterior region, between the suprasylvian sulcus and the sylvian sulcus, forms the transition zone between the parietal, the temporal, and the insular/perirhinal lobes (Fig. 2a). The presylvian sulcus departs from the rhinal fissure anteriorly (Fig. 1a, c) and separates the frontal lobe from the parietal lobe at the frontal end of the hemisphere together with the most anterior part of the coronal sulcus, (Fig. 2a, c). On the mesial side of the hemisphere one sees most rostroventrally the rostral sulcus, followed dorsocaudally by the genual sulcus located parallel to the anterior part of the corpus callosum, while the splenial sulcus is located closer to the dorsal surface posteriorly (Fig. 1d). The latter two sulci demarcate roughly the pericallosal lobe from the dorsally located frontal and occipital lobes (Fig. 2d). The retrosplenial sulcus separates partly the retrosplenial cortex from the anterior and ventrally located hippocampal structures (Figs. 1d, 2d), but is much better visualized after removal of the brain stem (Fig. 1f), where one also may appreciate how the retrosplenial sulcus ventrally and posteriorly is related to an indentation separating the temporal lobe from the occipital lobe and thus named the primitive occipitotemporal sulcus (Fig. 1f).

General inner structure of the minipig telencephalon

The inner structure of the minipig telencephalon is dominated by the ventricular system and white matter segregating telencephalic structures such as the basal ganglia, the claustrum, the amygdala, and the septum (Figs. 1e, g, 7; Figs. S1–S24).

The two lateral ventricles emerge as slit formed structures (the anterior part) at the level of the genu of the corpus callosum (Fig. S7). The lateral ventricle communicates at this point ventrally with its olfactory part, situated centrally in the olfactory bulb (Fig. 3a; Figs. S3–S7). The lateral ventricle enlarges dorsally at more posterior levels next to the septum pellucidum and forms here its central part (Figs. S8–S15). The communication to the diencephalic third ventricle occurs approximately at the

longitudinal mid level of the brain through the interventricular foramen of Monro. The central part of the lateral ventricle continues at posterior levels lateroventrally into its crescent shaped posterior part, situated lateral to the hippocampus and posterior medial to the amygdala (Fig. 7; Figs. S16–S21).

The main fiber systems of the minipig telencephalon are the corpus callosum (Fig. 1d, f, g; Figs. S7–S17), the anterior commissure (Fig. 1e; Fig. S12) and the hippocampal commissure (Fig. 1d, f; Figs. S15–S16), as well as the internal-, the external-, and the extreme capsules which, respectively, separate the caudate nucleus and the thalamus from the putamen, the putamen from the claustrum, and the claustrum from the insular/perirhinal cortex (Fig. 1e, g). Above the internal capsule, the white matter forms a prominent centrum semiovale/corona radiata (Figs. S5–S14), while the internal capsule caudally continues into the cerebral peduncle (Fig. 7; Figs. S16–S19). The cingulum can be depicted in myelin stained sections as it runs longitudinally through the pericallosal lobe dorsal to the callosal fibers while at anterior levels it has a vertical orientation deep to the cell layers of BA25 and the medial prefrontal cortex (Figs. S5–S18). The fimbria depart from the hippocampus and funnel anteriorly into the fornix, that gains a close relation to the anterior commissure (Figs. 1f, 4e; Figs. S12–S18). At the same coronal levels one may notice the more laterally situated stria terminalis approximating the lateral part of the anterior commissure to reach the bed nucleus of the stria terminalis (Fig. 1f; Fig. S12–S13). The diagonal band of Broca can be identified in the myelin stained sections as it curves around the most posterior part of the accumbens nucleus at the level of the transition between the taenia tecta and the septum (Figs. S9–S10).

The striatal complex comprising the caudate nucleus, the accumbens nucleus, and the putamen begins anteriorly lateral to the slit-like communication between the anterior and the olfactory part of the lateral ventricle (Fig. S7). At more posterior levels the internal capsule becomes more demarcated dividing the caudate nucleus and the putamen into two separate entities (Fig. 1g; Figs. S9–S15). Both structures fuse, however, ventrally, forming the large accumbens nucleus situated in the deep telencephalic gray at the level of the olfactory tubercle (Fig. 1e; Figs. S9–S12). The ventral pallidum occurs at the coronal level corresponding to the transition between the olfactory tubercle and the diagonal region (Figs. S12–S13). The ventral pallidum replaces thereby gradually the accumbens nucleus (Fig. S12) as it fills out the space between the bed nucleus of stria terminalis medially, the cortex of the diagonal region ventrally, and the putamen and the caudate nucleus dorsally. The ventral pallidum ends by definition at the level of the anterior commissure, as it, at more posterior levels, dorsally funnels into the globus pallidus located medially to the putamen (Figs. S13–S15).

Fig. 5 Microphotographs of selected parts of Nissl-stained coronal sections depicting the cytoarchitecture of the major areas of the pericallosal and perirhinal/insular lobes, while the indusium griseum (IG) can be seen in Fig. 3c and the agranular retrosplenial cortex (RSA) is depicted in Fig. 6h. Note that all images are shown at the same magnification. **a** Mesial part of Fig. S6 just below the corpus callosum depicting the Brodmann area 33 homolog cortex (BA33). **b** Ventromesial part of Fig. S7, depicting the subgenual cortex (BA25), *arrows* mark the characteristic white matter columns. **c** Mesial part of Fig. S6 dorsal to the corpus callosum depicting the anterior cingulate cortex (CgA). **d** Dorsomesial part of Fig. S13 depicting the posterior cingulate cortex (CgP). **e** Dorsomesial part of Fig. S21 depicting the granular retrosplenial cortex (RSG), *arrows* mark granules. **f** Ventrolateral part of Fig. S6 depicting the agranular ventral insula (AI). **g** Ventrolateral part of Fig. S6 depicting the the mid part of the insula (AI-GI). Ventrolateral part of Fig. S6 depicting the granular/dysgranular dorsal insula (GI). Ventrolateral part of Fig. S17 depicting the agranular perirhinal Brodmann area 35 cytoarchitectonic homolog cortex (PRh35). **j** Ventrolateral part of Fig. S17 depicting the granular/dysgranular perirhinal Brodmann area 36 cytoarchitectonic homolog cortex (PRh36)

The claustrum is large in the Göttingen minipig, anteriorly forming a ventrally located slit shaped structure (Fig. 1e), while at more posterior levels it has a more dorsal position and a thicker triangular shape (Fig. 1g). The claustrum consists of evenly distributed middle sized (20–25 μm) neurons (Fig. 5f, h) located deep to the insular/perirhinal cortex and lateral to the putamen, being separated from the latter by the external capsule (Fig. 1e, g; Figs. S5–S16).

The amygdala begins anteriorly at the level of the diagonal region, where it is located between the piriform cortex laterally and the diagonal region/olfactory tubercle medially (Fig. 1c). The posterior part of the amygdala is medially related to the fimbria and hippocampal formation (Figs. 1e, 4e), while it laterally approaches the piriform cortex and the piriform/entorhinal transition zone (Fig. 4e; Figs. S16–S18). A finer identification and segregation of the distinct nuclei within the amygdala awaits future studies combining histology and immunohistochemistry on coronal, sagittal and horizontal sections.

The bed nucleus of the stria terminalis is positioned close to the dorsolateral part of the anterior commissure and medial to the post commissural fornix, where it receives the stria terminalis (Figs. S12–S13). The bed nucleus of the stria terminalis is mainly formed by small (5–15 μm) densely packed cells that extend laterally and ventrally around the anterior commissure (Figs. S12–S13).

The septum is dorsally quite thin as it forms the septum pellucidum separating the central part of the lateral ventricles (Fig. 1d; Figs. S7–S17). The ventral broad cell rich part of the septum (Fig. 4d) has a more limited extent in the coronal plane as it begins behind the taenia tecta and

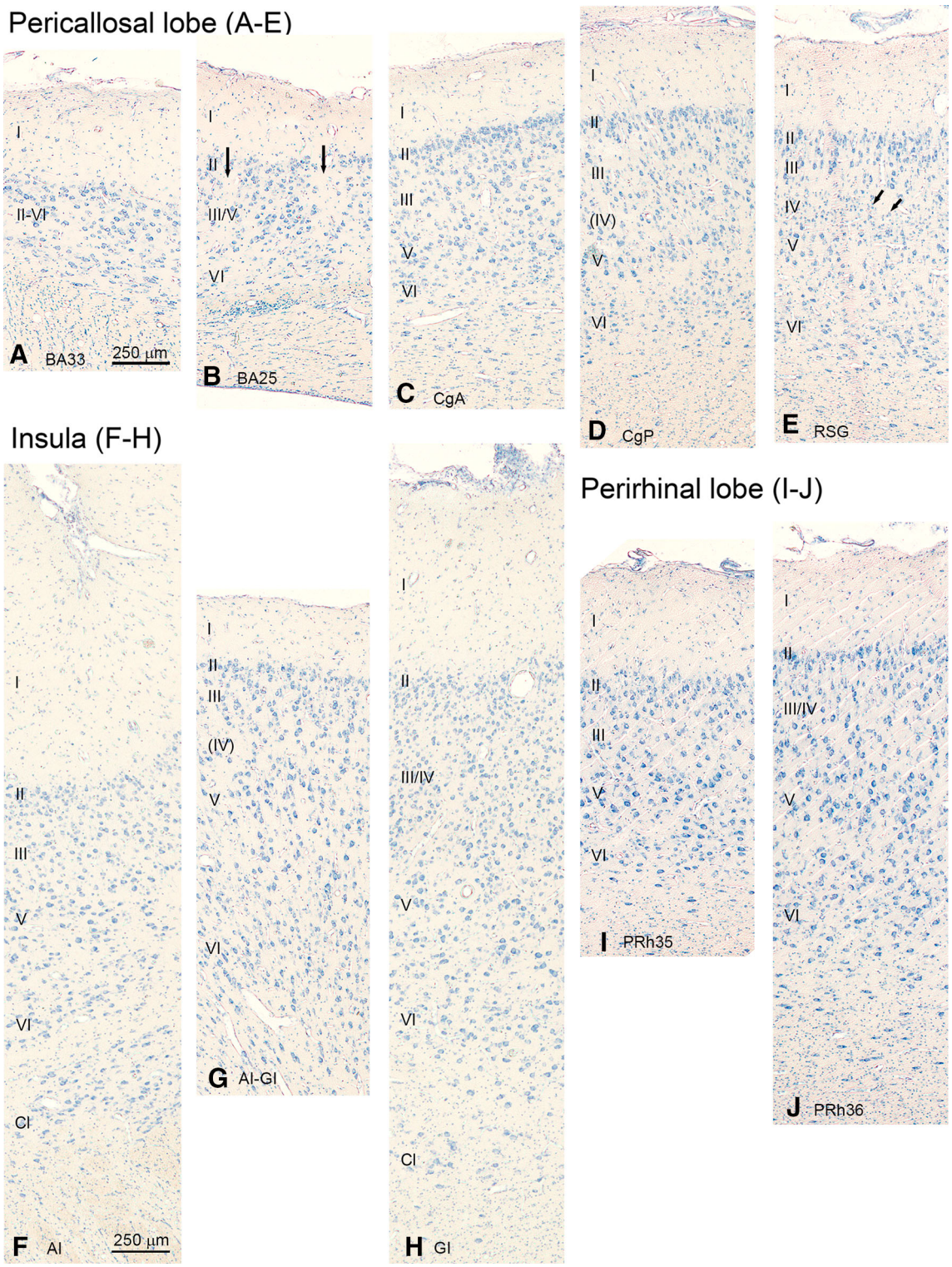
Pericallosal lobe (A-E)
I
II-VI
A BA33
250 µm
I
II
III/V
VI
B BA25
I
II
III
V
VI
C CgA
I
II
III
(IV)
V
VI
D CgP
I
II
III
IV
V
VI
E RSG
Insula (F-H)
I
II
III
V
VI
CI
F AI
250 µm
I
II
III
(IV)
V
VI
G AI-GI
I
II
III/IV
V
VI
CI
H GI
Perirhinal lobe (I-J)
I
II
III
V
VI
I PRh35
I
II
III/IV
V
VI
J PRh36

indusium griseum (Fig. S9), while posteriorly it is demarcated by the post commissural fornix passing through the rear part of the septum, and thus shaping the anterior limit of the interventricular foramen of Monro (Fig. S12). The septum harbors ventrally the anterior commissure (Fig. 1e), while ventrolaterally it is related to the bed nucleus of the stria terminalis (Fig. S12). The septum approaches anterior and ventrally the posterior dorsomedial part of the accumbens nucleus and the diagonal region (Figs. 1d–f, 2d). The septum contains several distinct cell clusters. It is thus possible to identify large (25–30 μm) loosely arranged neurons located in a central placed cluster around the midline (Fig. 4d). We name this area the medial septal complex. The medial septal complex is surrounded by smaller (5–15 μm) and more densely arranged cells filling the main part of the septum apart from a small dorsolateral located area, where larger (10–20 μm) loosely arranged cells are seen (Fig. 4d). These two areas form the lateral septal nuclear complex, which accordingly can be subdivided into a parvocellular and a magnocellular subarea (Fig. 4d; Fig. S11).

Cytoarchitecture of the subrhinal lobe

The olfactory bulb (Fig. 3a) is ventrally connected to the bony cribrosal lamina by the olfactory nerve layer, which dorsally ends in the glomerular layer of the olfactory bulb. Deep to the glomerular layer one encounters the thick external plexiform layer wherein single mitral cells can be seen now and then (Fig. 3a). The majority of the mitral cells form, however, a distinct but thin mitral cell layer of the olfactory bulb. Deep to the mitral cell layer one sees the internal plexiform layer and several broken rows of granule cells forming the granular cell layer of the olfactory bulb. The granule cells become more loosely arranged towards the subependymal cell layer and the ependyma, which surround the centrally located olfactory part of the lateral ventricle (Fig. 3a; Figs. S3–S9).

The accessory olfactory bulb is located on the mediodorsal side of the mid portion of the olfactory bulb (Fig. 3a; Fig. S4). The glomerular layer of the accessory olfactory bulb is less distinct, as the glomeruli are more closely arranged and surrounded by fewer cells (Fig. 3a). The external plexiform layer is thinner and the underlying mitral cell layer thicker as the mitral cells here do not form a single distinct cell layer. The granule cells of the accessory bulb also lack the tendency to form cell rows resulting in an even distribution of the granule cells of the accessory bulb (Fig. 3a). At the level of the accessory bulb one also notices the appearance of the anterior olfactory nucleus in the dorsal part of the bulb. The anterior olfactory nucleus has a three layered structure with a superficial molecular layer, a compact middle cell layer and a deep plexiform layer with loosely arranged cells (Fig. 3a, c; Fig. S4–S9). The anterior part of the anterior olfactory nucleus initially forms a cap like structure (Figs. S4–S5), while the middle cell layer at more posterior levels is separated into a medial and a lateral part by the olfactory part of the lateral ventricle (Fig. 3c; Figs. S6–S7). The lateral part of the anterior olfactory nucleus is laterally and dorsally separated from the three layered prepiriform cortex as the middle cell layer of the prepiriform cortex (Fig. 4a) is more demarcated because it contains larger (12–18 μm) and closely arranged densely stained cells (Figs. S6–S8). The medial part of the anterior olfactory nucleus is similarly medially and dorsally related to the taenia tecta, which like the prepiriform cortex has a three-layered structure although the middle cell layer is thinner (Fig. 3c; Figs. S7–S8). Posteriorly the middle cell layer of the anterior olfactory nucleus becomes less dense and forms here a more homogeneous collection of cells located interposed between the dorsally emerging accumbens nucleus and the ventrally emerging olfactory tubercle (Fig. S9). Mesial and dorsally the tenia tecta initially approaches the medial prefrontal cortex (Fig. 3c), while at more posterior levels it fuses into the indusium griseum (Fig. S9).

The olfactory tubercle has three layers named the plexiform layer, the pyramidal cell layer and the polymorph cell layer (Fig. 3b; Figs. S9–S12). The pyramidal cell layer is easily recognizable as it has an irregular wavy localization with more or less densely arranged pyramidal cells of varying size (5–20 μm), probably reflecting the shrunken unordered tubercular surface (Fig. 3b). The deep polymorph layer is generally less well defined, but contains at varying locations aggregations of either large (20–30 μm) loosely arranged cells, or smaller (<5 μm) more densely packed granular cells which could correspond to the islands of Calleja and accordingly has been depicted as such (Fig. 3b). In the superficial fiber rich plexiform layer one occasionally notices submeningeal collections of very small (≪5 μm) densely packed granule cells, which also have been described previously in other mammals (Cajal 1904).

The diagonal region is interposed between the olfactory tubercle anteriorly, and the hypothalamus and the amygdala posteriorly, while it laterally approaches the prepiriform cortex. The cells of the diagonal region are large (20–30 μm) and very loosely arranged without any obvious stratification, resulting in a pale and anonymous appearance (Fig. 4c; Fig. S13). The appearance of a dense layer II in the middle of the diagonal region marks the nucleus of the lateral olfactory tract, and thus the beginning of the amygdala (Fig. S14).

The cytoarchitecture of the pig hippocampal formation has previously been elaborately described (Holm and Geneser 1989, 1991a, b). We have, accordingly, in our

Nissl stained sections been able to segregate the hippocampal formation into a fascia dentatae, a fasciola cinereum, a hippocampus with CA3- and CA1 subregions, a subiculum, a presubiculum, a parasubiculum and an entorhinal area (Fig. 4e). The fascia dentatae contains a molecular and a granular layer, while the dentate hilus region, especially in horizontal sections, can be segregated into a thin subgranular outer plexiform layer and an evenly thin outer cell layer separated by a more prominent inner plexiform layer and inner cell layer (Fig. 4e). The fasciola cinereum is derived from the fascia dentatae and has a ventral position just next to the splenium of corpus callosum (Fig. S17). The hippocampus is divided into a CA3- and a CA1 area based on the appearance of a stratum lucidum (the layer located apical to the pyramids in CA3 and targeted by the mossy fibers) and the thickness of the pyramidal layer (thicker and more loosely arranged in CA3) (Fig. 4e). In the subiculum the pyramids of the pyramidal layer form a thick loose cell layer surrounded by a superficial fiber rich plexiform layer and a deep dorsal psalterium giving rise to the hippocampal commissure (Fig. 4e). The presubiculum can be segregated from the subiculum by the appearance of a distinct thin cell layer (layer II) superficial to the more loosely arranged deeper cell layers (Fig. 4e). The parasubiculum has a very limited extent (around 2 mm and thus only visible on supplementary atlas figures S21 and S22) and will accordingly not appear on many sections through the hippocampal formation. It is characterized by dense Nissl stained pyramidal neurons which form a homogenous layer II–III that is less clearly separated from the deeper cell layers compared to the neighboring presubicular and entorhinal cortices (Fig. 4e; Figs. S21–S22). The entorhinal area is characterized by a clustering of the cells in layer II, as well as a bright separation (lamina dissecans) between the superficial cell layers (layer II and III, here together named the external lamina) and the deeper located cells in the internal lamina comprising layer IV–VI (Fig. 4e). This separation becomes more clear in the lateral entorhinal area where the cells of both laminae are larger (20–30 μm), in contrast to the smaller (15–20 μm) and more densely arranged cells in the medial entorhinal area (Fig. 4e).

Cytoarchitecture of the pericallosal lobe

The cortex of the pericallosal lobe has a varied cytoarchitecture and can thus be divided into four major areas named the subgenual cortex (Brodmann area 25 cytoarchitectonic homolog cortex, BA25), the anterior agranular cingulate cortex, the dysgranular posterior cingulate cortex and the granular retrosplenial cortex (Fig. 2d), and three minor areas named agranular retrospenial cortex, Brodmann area 33 cytoarchitectonic homolog cortex (BA33) and indusium griseum. The subgenual cortex is thin, agranular and with no clear distinction between the medium sized (15–20 μm) neurons in layers III and V (Figs. 3c, 5b; Table 2). Layer II consists of two to three rows of compactly arranged small sized (10–15 μm) neurons, whereas layer VI is thin and has loosely distributed evenly sized (∼15 μm) neurons (Fig. 5b). Most characteristic for this area, cell poor columns of white mater run perpendicular to the pial surface from layer I into layer II and the upper part of layer III/V, thus segregating the superficial cell layers into separate columnar clusters (Figs. 3c, 5b). The subgenual cortex increases in thickness anteriorly and ventrally, where the superficial columnar cell pattern likewise disappears and is thereby converted into the medial prefrontal cortex (Fig. 3c). The subgenual cortex, on the other hand, becomes thinner and looses cortical lamination posteriorly and dorsally, as it gradually is transformed to area BA33 (Figs. 3c, 5a), which has no clear cortical lamination. The uniformly lightly stained neurons (∼15 μm) of area BA33 will finally narrow into the indusium griseum, an area with a single cell layer (Fig. 3c). These two areas cover, accordingly, the anterior border of the septum and the outer surface of the corpus callosum from the lamina terminalis to the retrosplenial sulcus (Figs. S6–S18). The anterior cingulate cortex constitutes the anterior dorsal part of the pericallosal lobe (Fig. 2d). It resembles the more frontally located medial prefrontal cortex of the Göttingen minipig, as it is agranular and without major difference in size and arrangement of the 20–25 μm sized neurons of layers III and V, whereas the cells of layer II are more densely aligned and thus clearly demarcate this layer (Fig. 5c; Table 2). As one moves posteriorly through the cingulate gyrus, the thickness of the cingulate cortex increases, while the cells of layer III become smaller (∼15 μm) and more widely dispersed. The larger (20–25 μm) cells of layer V can now be clearly segregated, forming a superficial cell dense layer Va and a deeper cell poor zone Vb, towards the evenly sized (∼15 μm) cells of layer VI, which also increase in thickness (Fig. 5d). The cingulate cortex at these more caudal levels has a dysgranular appearance, as indicated on Fig. 5d, and is accordingly named the posterior cingulate cortex. A real granular layer is, however, first seen in the granular retrosplenial cortex, were several rows of very small (<5 μm) granules push the evenly sized (12–18 μm) and stained neurons of layers II and III together, while layers V and VI are thick and contain widely dispersed medium sized (15–20 μm) cells (Fig. 5e). The granular retrosplenial cortex is generally, due to its prominent granular layer IV, sharply separated from the neighboring hippocampal formation, area BA33, and from the posterior cingulate- and motor cortices, whereas towards the occipital lobe there is a more gradual decrease in cortical

thickness, and in the number and rows of granule cells (Fig. 6h). One may thus define a retrosplenial agranular cortex situated between the retrosplenial granular cortex and the peristriate cortex, lacking the prominent rows of granules of the retrosplenial granular cortex, and the more prominent layer V cells and well segregated layer II and III of the peristriate cortex (Fig. 6h).

Cytoarchitecture of the perirhinal/insular lobe

The perirhinal/insular lobe is located on the lateral side of the hemisphere forming a transition zone between the allo- and palaeocortical subrhinal lobe, and the dorsally located neocortical parietal and temporal lobes (Fig. 2a). The anterior part of the perirhinal/insular lobe is formed by the insula (Figs. S4–S16), while the perirhinal region constitutes the posterior part (Figs. S17–S24). Both regions can further be subdivided into an agranular ventral part encompassing the agranular ventral insular cortex and the perirhinal Brodmann area 35 cytoarchitectonic homolog cortex, and a dorsal thicker part encompassing the granular dorsal insular cortex and the dysgranular perirhinal Brodmann area 36 cytoarchitectonic homolog cortex. The agranular ventral insula has a thick layer I (Fig. 5f; Table 2). Layers II, III, and V are thin, and their cells are loosely arranged, so that a distinct layering is less obvious although cell size increases from layer II to layer V. Layer VI has a similar thickness, and loosely arranged but slightly smaller cells compared to layer V (Fig. 5f; Table 2). The thickness and cell density in layer III increases as one moves dorsally (Fig. 5g, h), giving the dorsal insula a granular/dysgranular appearance, although no distinct granules (like those seen in retrosplenial granular cortex) can be identified. The cells in the dorsal insula are still loosely arranged, and the difference in cell-size and staining intensity vary only slight between layers II–VI, thus making a sharp segregation of the different layers difficult (Fig. 5h). The agranular perirhinal cortex is similar to the agranular insula, although the cells seem to be a little bit more intensely stained and packed together, thus making identification of layers II–VI more easy (Fig. 5i; Table 2). The dorsally located granular perirhinal cortex has a thicker cortex due to the expansion of layer III, which may appear dysgranular, and layer V, which can be divided into a cell rich superficial part Va and a deeper cell poor part Vb (Fig. 5j; Table 2). Layer VI is likewise considerably larger in the granular perirhinal cortex (Fig. 5j) compared to the ventrally located agranular perirhinal cortex (Fig. 5i).

Cytoarchitecture of the frontal lobe

The frontal lobe cortex can in general be divided into two major subfields termed the motor cortex and the prefrontal cortex (Fig. 2). The prefrontal cortex is agranular and characterized by a very gradual transition between the pyramidal cells of layers III and V (Fig. 6a; Table 2). The pyramidal cells of layer II are closely aligned, forming a thin demarcated layer in contrast to the underlying slightly larger (20–25 μm) and more loosely arranged pyramidal cells of the thick layers III–V. Layer V of the prefrontal cortex can furthermore be divided into a more cell dense superficial layer Va and a deeper layer Vb where the pyramidal cells are very loosely arranged. Layer VI consist of smaller (15–20 μm) and more densely packed cells separating it from the overlying layer Vb (Fig. 6a). On pure topographical grounds the prefrontal cortex is divided into a medial, a ventral and a lateral part, occupying the medial, ventral and lateral surface of the frontal hemisphere. The medial prefrontal cortex will caudally and dorsally be related to the agranular anterior cingulate cortex which has a similar cytoarchitecture, and the subgenual cortex which is thinner and characterized by the clustering of the pyramidal cells in layer II, while it caudally and ventrally approximates the compact cell layer of the taenia tecta (Figs. 2, 3c).

The motor cortex occupies the dorsoposterior part of the frontal lobe (Fig. 2). The motor cortex is an agranular cortex characterized by large (35–45 μm) layer V pyramidal cells (Fig. 6b; Table 2). This feature distinguishes it from the thicker "granular" somatosensory cortex of the parietal lobe (Fig. 6c, d; Table 2), as well as from the more homogeneous and agranular prefrontal and anterior cingulate cortices (Figs. 5c, 6a; Table 2). At the transition to the somatosensory cortex of the parietal lobe, the visual cortex of the occipital lobe, and the retrosplenial cortex of the pericallosal lobe, the motor cortex becomes increasingly cell dense in the deep part of layer III, where increasing amounts of smaller (15–20 μm) cells appear, while the layer V pyramidal cells become less prominent, thus assuring a gradual transition to these neighboring cortices.

Cytoarchitecture of the parietal lobe

The parietal lobe occupies the anterior laterodorsal surface of the hemisphere (Fig. 2a, b). It has a six-layered cortex that can be subdivided into two subareas, named the ventral and the dorsal somatosensory cortex. The dorsal somatosensory cortex is characterized by a high number of evenly stained small to medium sized (10–18 μm) cells located in layers II, III and IV which only can be segregated into their laminae by the slightly looser arrangement of the layer III cells (Fig. 6d). The cells of layer V are a bit larger (15–20 μm), forming a thin superficial stripe of densely arranged cells (Va) and a wider deeper row of more widely dispersed cells (Vb), that are gradually replaced by the slightly smaller and more condensed but still loosely arranged cells of layer VI

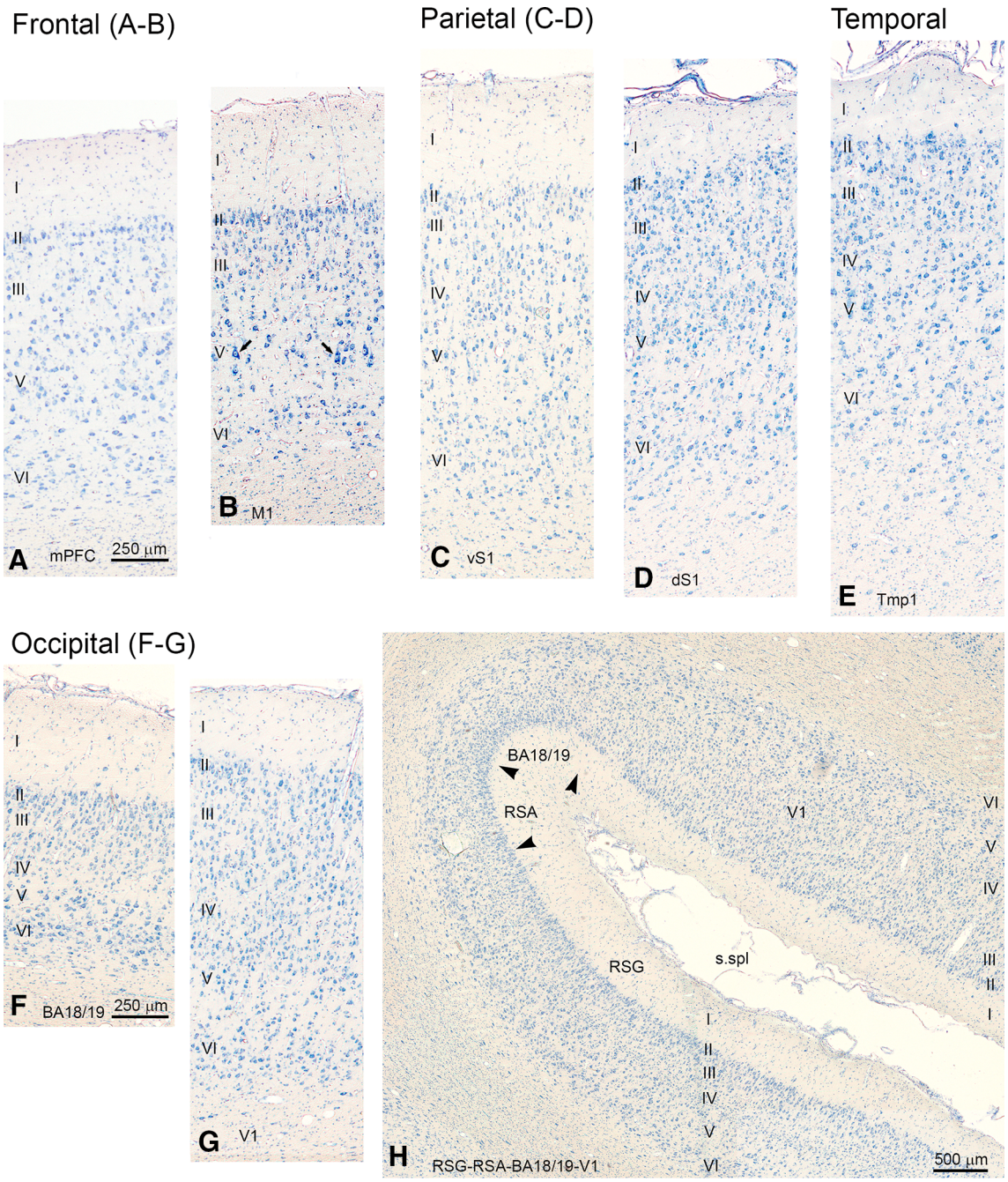

Fig. 6 Microphotographs of selected parts of Nissl-stained coronal sections depicting the cytoarchitecture of the frontal, the parietal, the temporal and the occipital lobes. Note that all images, apart from Fig. 6h, are at the same magnification. **a** Mediomesial part of Fig. S3 depicting the medial prefrontal cortex (mPFC). **b** Dorsomesial part of Fig. S4 depicting the frontal motor cortex (M1), *arrows* indicate the characteristic layer V pyramids. **c** Mediolateral part of Fig. S6 depicting the ventral parietal somatosensory cortex (vS1). **d** Dorsolateral part of Fig. S8 depicting the dorsal parietal somatosensory cortex (dS1). **e** Mediolateral part of section#1825 (located between Figs. S18 and S19) depicting the temporal cortex (Tmp1). **f** Dorsomesial part of Fig. S13 depicting the peristriate cortex (BA18/19). **g** Mediodorsal part of Fig. S21 depicting the striate cortex (V1). **h** Low-magnification image of dorsomesial part of Fig. S21 depicting the transition between the striate (V1), peristriate (BA18/19), agranular retrosplenial (RSA) and granular retrosplenial (RSG) cortices

(Fig. 6d). Ventrally in the parietal lobe the cells of layers II–VI are lined up in a columnar radial arrangement, which combined with a slightly lower cell density, gives this cortex a much clearer lamination. This area is furthermore characterized by a thicker layer I, and thus named the ventral somatosensory cortex (Fig. 6c).

Cytoarchitecture of the temporal lobe

The cortex of the temporal lobe is thick and has a laminar pattern similar to that of the parietal cortex, although the cells are fewer in all layers (Fig. 6e). One notes especially the coarse pyramids (15–22 μm) of layer V and the loosely arranged cells forming the broad layer VI (Fig. 6e; Table 2).

Cytoarchitecture of the occipital lobe

The occipital lobe (Fig. 2a, b, d) can be divided into a major central part named the striate cortex, surrounded by a thin transition zone towards the retrosplenial (Fig. 6h) and temporoparietal cortices named the peristriate cortex. The striate cortex has a similar lamination pattern as the parietal and temporal cortices, but the cells are a bit smaller (10–15 μm) and more compactly arranged giving this cortex a very cell dense appearance (Fig. 6g; Table 2). Layer IV has a considerable thickness, with small (10–12 μm) cells arranged in a random manner (Fig. 6g), although definite granules as seen in the granular retrosplenial cortex (Figs. 5e, 6h) cannot be identified. Layer VI is thinner compared to the other sensory cortices, but still separated from the larger (12–18 μm) pyramids of layer V by a cell poor layer Vb (Fig. 6g). Interestingly, the myelin stained sections displayed a clear line of Gennari, corresponding to the extent of the striate cortex (Fig. 7d). The peristriate cortex has only half to 2/3 the thickness of the striate cortex, although layer I is thicker (Fig. 6f, h). All the cellular layers are thus reduced in size, and layer V can no longer be subdivided in to sublayers Va and Vb (Fig. 6f).

Discussion

This study provides a detailed description of the cytoarchitecture and surface anatomy of the Göttingen minipig telencephalon based on macrophotos and direct microscopy of consecutive Nissl-stained coronal sections. We had also access to similar myelin-stained coronal sections, but apart from the demonstration of a prominent line of Gennari in the striate cortex (Fig. 7d), these were not useful for further segregation of the cerebral cortex, in contrast to their usefulness in the identification of subcortical brain structures and fiber tracts (Larsen et al. 2004; Ettrup et al. 2010). We can, however, not exclude that a conventional myelin stain based on luxol fast blue or immunohistochemistry might reveal a more detailed cortical myelin staining pattern.

The cytoarchitecture and surface anatomy of the pig cerebral cortex have previously been elaborately described (Campbell 1905; Stephan 1951; Ariëns Kappers et al. 1967) and more superficially dealt with (Brodmann 1909; Kruska 1970; Jelsing et al. 2006a), just as two MR-based 3D segregations of the pig brain have been presented (Watanabe et al. 2001; Saikali et al. 2010). However, none of these studies present consecutive delineated sections through the pig brain as seen in stereotaxic atlases. The known cytoarchitectural stereotaxic pig brain atlases have on the other hand not included any cortical delineations (Yoshikawa 1968; Salinas-Zeballos et al. 1986; Fèlix et al. 1999). We find, accordingly, that an updated coherent cytoarchitectonic description and delineation of the Göttingen minipig telencephalon, supplemented with 24 consecutive high-magnification coronal sections forming a cytoarchitectonic atlas of the Göttingen minipig cerebrum accessible on http://www.cense.dk/minipig_atlas/index.html, would be beneficial for future neuroscientific research in this promising non-primate large animal model. Although the supplementary atlas images and the two abbreviation lists are not incorporated directly into the current paper, we find the presented web-based atlas advantageous, as it allows the viewer to examine the 24 coronal levels depicted in Fig. 7a, b both at a low magnification for whole section overview and at subsequent high magnifications for visualization of the distinct cytoarchitecture of the individual depicted telencephalic areas.

Like human brains, pig brains are not all alike, as they keep growing through life and furthermore present individual and subspecies differences in size and sulcal surface pattern (Herre 1936; Stephan 1951; Lunau 1956; Kruska 1970, 1972; Kruska and Stephan 1973; Hadziselimovic and Dilberovic 1977; Plogmann and Kruska 1990; Jelsing et al. 2006b). The Göttingen minipig brain may in that context be considered to be rather small in absolute terms. It weighs approximately only 50% of the similar one year old Danish landrace pig brain, although the relative brain size is larger, as the adult landrace pig weigh more than 100 kg, whereas the minipig kept on diet will weigh around 25 kg (see also Table 1; Jelsing et al. 2006b). The sulcal pattern of the Göttingen minipig is quite consistent when it comes to the genual, splenial, retrosplenial, lateral, suprasylvian, sylvian, presylvian, sagittal, and semiannular sulci, which generally can be identified in all pig subspecies (Herre 1936; Stephan 1951; Kruska 1970, 1972; Kruska and Stephan 1973; Hadziselimovic and Dilberovic 1977; Plogmann and Kruska 1990; Jelsing et al. 2006a). Several minor sulci may develop around the former mentioned sulci and may furthermore increase in number and conspicuity as the animal grows. These sulci are, therefore, not named or dealt with in the present work. One sulcal variation is, however, consistently found in pigs in general. Thus, the coronal sulcus may continue posterior and mesially (Fig. 8) to the junction between the dorsally located ansate sulcus and the mesially located cruciate

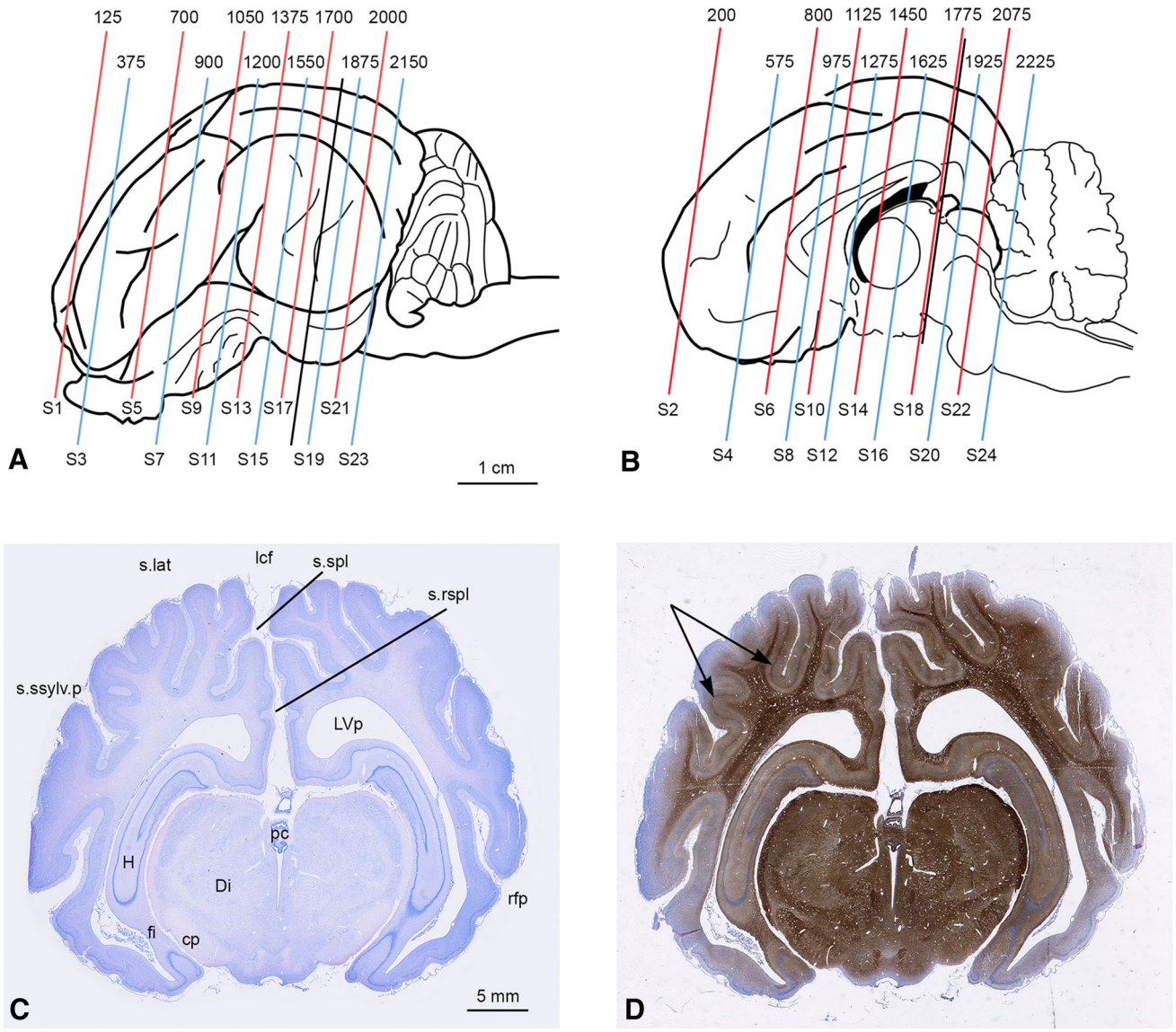

Fig. 7 Schematic drawings (AB) of the Göttingen minipig brain corresponding to views shown in Figs. 2a and 2d, respectively, depicting the section plane and position of the high-resolution atlas images presented as supplementary material on http://www.cense.dk/minipig_atlas/index.html. Note that the section number is depicted above the section plane line, and that the number of sections and thus the distance between the *lines* is not the same from section to section. The *numbers* below the section plane line depict the supplementary figure number. The *black* section plane line marks the position of **c**, **d**, which are Nissl- and Myelin-stained coronal sections #1800 and #1801, respectively. Note the prominent line of Gennari (*arrow*) in the striate cortex on **d**. *cp* cerebral peduncle, *Di* diencephalon, *fi* fimbria, *H* hippocampus, *lcf* longitudinal cerebral fissure, *LVp* lateral ventricle posterior part, *pc* posterior commissure, *rfp* rhinal fissure posterior part, *s.lat* lateral sulcus, *s.rspl* retrosplenial sulcus, *s.spl* splenial sulcus, *s.ssylv.p* suprasylvian sulcus posterior part

sulcus (Herre 1936; Stephan 1951; Kruska 1970; Hadziselimovic and Dilberovic 1977). To increase confusion, the ansate sulcus depicted by us is not defined by Stephan (1951) or Kruska (1970), but instead named the cruciate sulcus. The ansate sulcus may likewise, not always be directly continuous with the coronal sulcus, but instead anteriorly dispatch a branch that runs lateral and parallel to the posterior part of the coronal sulcus (Stephan 1951; Kruska 1970). These common variations are important to know, as the ansate and cruciate sulci, identified and depicted by us, separates the frontal and parietal lobes from the posteriorly located occipital lobe, and the coronal sulcus similarly separates the medially located motor cortex from the laterally located parietal lobe. The ansate-, cruciate- and coronal sulci are thus partly considered to be the homologs of the human central sulcus, although the coronal sulcus in subprimates has a more sagittal orientation (and thus not coronal) due to the minor development of the non

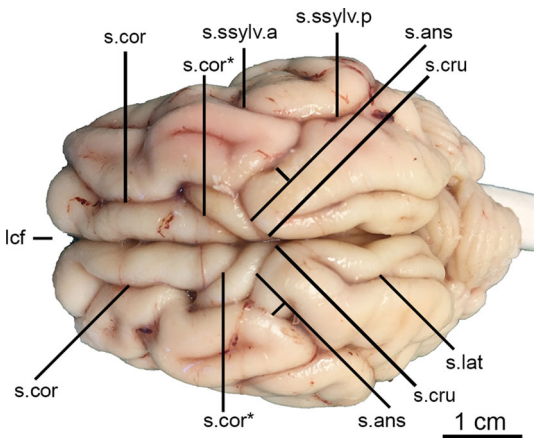

Fig. 8 Photographic illustration of the mediodorsal telencephalic sulcal pattern seen on a 15 month old female Göttingen minipig included in an on-going tracing study on the pyramidal tract. Note, how the coronal sulcus (s.cor) in this animal (compared to Fig. 1b) continues posteriorly and mesially (s.cor*) in front of the dorsally located ansate sulcus (s.ans) and the mesially located cruciate sulcus (s.cru). *lcf* longitudinal cerebral fissure, *s.cor* coronal sulcus, *s.lat* lateral sulcus, *s.ssylv.a* suprasylvian sulcus anterior part, *s.ssylv.p* suprasylvian sulcus posterior part

motor part of the frontal lobe (Ariëns Kappers et al. 1967). Within the occipital lobe the lateral sulcus has a similar sagittal orientation as the coronal sulcus (Figs. 1b, 2b). The lateral sulcus is also named the marginal sulcus (Sisson and Grossman 1956; Igarashi and Kamiya 1972), which in our opinion is a better name, as it avoids confusion with the sylvian sulcus, which generally is named as the lateral sulcus/fissure in modern human neuroanatomy (Bjarkam 2015). Given the nomenclature arguments presented previously we have, however, chosen to adhere strictly to the nomenclature established by Ariëns Kappers et al. (1967).

The cytoarchitecture of the Göttingen minipig subrhinal lobe is very characteristic and easy to delineate, probably due to the prominent development of the pig olfactory system. These regions have previously been described in detail in pigs (Stephan 1951; Lunau 1956; Herec 1967; Kruska 1970; Kruska and Stephan 1973; Holm and Geneser 1989, 1991a, b), and we have generally not much to add, apart from the fact, that this study for the first time presents a full delineation of the subrhinal lobe in consecutive coronal sections. This is especially noteworthy for the hippocampal formation, as this structure is generally presented in horizontal sections (Holm and Geneser 1989, 1991a, b), where the transition between the different subfields is easier to segregate (Fig. 4e). The finer segregation of the pig amygdala and septum into distinct subnuclei awaits further studies using histo- and immunohistochemistry, and has accordingly not been added to current work.

The cytoarchitecture of the neocortical pericallosal, insular/perirhinal, frontal, parietal, temporal and occipital lobes display likewise several specific features (Table 2) that allow the current microscopy-based cytoarchitectonic segregation of the Göttingen minipig neocortex (Fig. 2). The cells of the pig neocortex are, however, in general much alike when it comes to size and shape (Figs. 5, 6). Thus, apart from the small granules (<5 µm) of the retrosplenial granular cortex (Fig. 5e; Table 2), typical layer IV granules are difficult to identify with certainty. Likewise, the pyramids of the motor cortex are large (35–45 µm) (Fig. 6b; Table 2), but to classify them as Betz's cells (Saikali et al. 2010) would definitely be an overstatement, which also has been noted by Campbell (1905) and Stephan (1951). The difference between the agranular and the granular pig cortex is, accordingly, mainly found in the cellularity of layers III and IV, and in the similarity in size of the cells in layers III and V. Thus, agranular cortex has fewer and less densely arranged cells in layers III and V (Figs. 5b, c, f, g, i, 6a, b; Table 2), and apart from in the motor cortex (Fig. 6a), these two layers mingle inconspicuously with each other. Granular cortices (Figs. 5e, h, j, 6c–g; Table 2) are on the other hand more cell rich, especially in layers III-IV, which are dominated by medium to small sized pyramidal cells, and these cortices are thus in general thicker and more cell dense than the agranular cortices (Figs. 5, 6). Thus, our attempt to homologize some pig brain areas (BA18/19, BA25, BA33, PRH35, PRH36) to similar defined Brodmann areas and some pig brain areas [motor (M1), visual (V1), somatosensory (dS1, vS1)] to functionally defined cortices is purely based on cytoarchitecture and topology, and does not reflect further immunohistochemical, connectional or functional studies that may result in a more detailed or precise segregation. We hope, however, that the current work may serve as the foundation for such future studies.

The pericallosal lobe is anteroventrally differentiated as the subgenual cortex. This cortex with its characteristic superficial white matter columns (Figs. 3c, 5b) was originally identified based on cytoarchitecture by Brodmann (1909), and has in the pig previously been described as area 25 by Stephan (1951) and as infralimbic cortex by Jelsing et al. (2006a). It might likewise represent the major part of Campbell's area limbic A (1905). The cingulate cortex with its agranular anterior part (Fig. 5c) and dysgranular posterior part (Fig. 5d) was depicted by Campbell (1905) as limbic, and by Stephan (1951) as area 24. Jelsing et al. (2006a) describe the close resemblance of the anterior part of the cingulate cortex to their prefrontal cortex, and also demonstrate how this area is related to the mediodorsal thalamus by fiber connections. The retrosplenial granular cortex (Fig. 5e), which correspond, to area limbic B of Campbell (1905), area 30/31 of Stephan (1951), and the dorsal posterior cingulate cortex of Saikali et al. (2010), has a wide extent on the posterior mesial side of the

hemisphere (Fig. 2d), where it caudally is sharply segregated from the hippocampal structures both in cytoarchitecture and by the retrosplenial sulcus, whereas the anterior transition to the dysgranular posterior cingulate cortex is more gradual.

The perirhinal/insular lobe cytoarchitecture (Fig. 5f–j) represents a transition from the ventrally located allo- and palaeocortical subrhinal lobe to the six-layered neocortex seen in the dorsally located parietal and temporal lobes (Fig. 2). One moves accordingly from agranular (Fig. 5f, i) to thicker dysgranular/granular cortices (Fig. 5h, j; Table 2) as one moves dorsally through this lobe, which generally corresponds to the extra-rhinic cortex of Campbell (1905) and to area 13–16 and area 36 of Stephan (1951). Jelsing et al. (2006a) delineate three anterior insular areas, where their ventral and medial areas correspond to our agranular- and granular insula, respectively, whereas their most dorsal area in our opinion rather should be allocated to the parietal lobe cortex, as this area displays a full six-layered cortex (Fig. 6c) and not is directly related to the claustrum, which has a more medioventral position (Figs. S4–S16). It is furthermore noteworthy, that the ventral and medial insular areas, but not the dorsal anterior insular area, in the latter study, have prominent fiber connections to the mediodorsal thalamic nucleus (Jelsing et al. 2006a).

The frontal lobe cytoarchitecture is for the main part delineated as motor cortex (Fig. 2) although the anterior transition to the agranular prefrontal cortex is gradual, and thus should be taken with caution. The position of the motor cortex has caused some confusion since the study of Campbell (1905), who admittedly described problems with the segregation due to the lack of Betz cells. Campbell (1905) places, accordingly, the motor cortex more anterior and only on the laterodorsal side of the hemisphere, while the sensory cortex is located posteriorly and the parietal cortex mesially to the motor cortex. Our cytoarchitectonic parcellation of the frontal lobe (Fig. 2) is in full accordance with that Stephan (1951) and with the comparative studies of Ariëns Kappers et al. (1967). Functionally, it is supported by tracing studies on the pyramidal tract (Palmieri et al. 1987) and the MR/histology based delineation of the domestic pig primary motor and premotor cortex (Saikali et al. 2010). The frontal pole is covered by agranular cortex without a clear distinction between the cells of layers III and V (Fig. 6a). We have topographically subdivided this area into a medial, a ventral and a lateral portion (Figs. S1–S7) which grouped together are encompassed in the mediopolar frontal cortex and the anterior parts of the dorsomedial and dorsolateral frontal regions of Jelsing et al. (2006a), who likewise describe prominent fiber connections between these areas and the mediodorsal thalamus. Like Jelsing et al. (2006a) and Saikali et al. (2010), we do not identify a granular prefrontal area, which according to the comparative studies of Ariëns Kappers et al. (1967) should be located ventral and anterior to the presylvian sulcus in some ungulates. Stephan (1951) identified a granular frontal area 8 which has the same extent as our agranular prefrontal cortex, and mentions on page 545 that "The cortex is of intermediate thickness and composed of intermediate and large sized cells; small number of granules, no columnar cell organization; poorly differentiated lamination (author's translation)", thus confirming the problems with a firm classification of this area. Campbell (1905) delineates a frontal area of same extent as Stephan's (1951) area 8, but does not offer any specific comments on the granularity of the depicted area.

The parietal lobe with its somatosensory areas (Fig. 6c, d) occupies the anterior laterodorsal surface of the pig hemisphere (Fig. 2), which generally has been substantiated by several neurophysiological studies (Woolsey and Fairman 1946; Andrews et al. 1990; Craner and Ray 1991a, b) and the cytoarchitectonic studies of Campbell (1905), Stephan (1951), Jelsing et al. (2006a) and Saikali et al. (2010). It is, however, noteworthy that our segregation continues more ventrally towards the rhinal sulcus, as we include the main anterior part of the ectosylvian B area of Campbell (1905) corresponding to the main dorsal part of area 13–16 of Stephan (1951) and the dorsal part of the anterior insula of Jelsing et al. (2006a) and Saikali et al. (2010) into our somatosensory parietal lobe, as we find the six layered structure of our ventral somatosensory cortex (Fig. 6c) in more resemblance to the sensory cortices of the dorsal somatosensory cortex (Fig. 6d) and the temporal cortex (Fig. 6e). We do hereby get a closer resemblance to the cytoarchitectonic (Rose 1942) and connection based (Dinopoulos et al. 1985) segregation of the sheep brain, while we at the same time recognize the difference in fiber connections and the lacking relation to the claustrum of this area discussed previously under the cytoarchitecture of the perirhinal/insular lobe.

The temporal lobe cortex (Fig. 6e) is located between the posterior part of the suprasylvian sulcus and the ventrally located perirhinal/insular lobe (Fig. 2) constituting the posterior half of the ectosylvian B area of Campbell (1905), while his ectosylvian A area in our opinion represents a transition zone between the parietal, temporal and insular cortices. Our cytoarchitectonic segregation of the temporal "auditory" cortex is in strict accordance with the delineation of area 20–22 by Stephan (1951) and the auditory cortex of the European wild boar (Plogmann and Kruska 1990). It is also in accordance with the temporal and auditory cortices delineated by Saikali et al. (2010) in the domestic pig, and is furthermore supported by electrophysiological recordings of auditory evoked potentials (Woolsey and Fairman 1946; Andrews et al. 1990).

The occipital lobe covers the dorsoposterior part of the minipig hemisphere (Fig. 2). It has a well developed and distinct cytoarchitecture that allowed us to identify a large striate cortex (Fig. 6g, h), surrounded in the periphery by a thinner peristriate cortex (Fig. 6f, h). The striate cortex displayed furthermore a prominent line of Gennari on myelin stained sections (Fig. 7d), which is the most conspicuous myeloarchitectonic feature of the minipig cortex. The location and cytoarchitecture of the minipig occipital lobe are in full accordance with the findings of Campbell (1905), Stephan (1951) and Kruska (1972) and likewise similar to that of the sheep brain (Rose 1942). We were generally also in accordance with the findings of Saikali et al. (2010), although we not were able to separate the peristriate cortex into a distinct V2 and a distinct V3 area. It is interesting that functional studies with fMRI (Fang et al. 2006) have suggested that the pig, like primates, may process a dorsal magnocellular and ventral parvocellular stream within the visual cortex. Further cortical tracing studies might, accordingly, lead to a more detailed segregation of the minipig striate cortex into specific visual fields.

In conclusion, this paper, together with the atlas images presented on http://www.cense.dk/minipig_atlas/index.html, provides a detailed cytoarchitectonic account of the Göttingen minipig telencephalon, that not only may support future translational studies examining the impact of new neurosurgical treatment modalities (Bjarkam et al. 2008b, 2010; Fjord-Larsen et al. 2010; Sørensen et al. 2011), but also may prove to be a framework for future neural tracing, and immuno- and histochemical studies on the minipig cerebral cortex, allowing us to refine the currently provided knowledge on the ungulate telencephalon.

Acknowledgements The authors acknowledge with gratitude the skillful assistance of Mrs. F. Gün, Ms. D. Jensen, Ms. K. S. Bech and Mr. A. Meier. The Danish Medical Research Council, and the Lundbeck Foundation supported financially the study.

References

Andersen F, Watanabe H, Bjarkam CR, Danielsen EH, Cumming P, The DaNeX Study Group (2005) Pig brain stereotaxic standard space: mapping of cerebral blood flow normative values and effect of MPTP-lesioning. Brain Res Bull 66(1):17–29

Andrews RJ, Knight RT, Kirby RP (1990) Evoked potential mapping of auditory and somatosensory cortices in the miniature swine. Neurosci Lett 114:27–31

Ariëns Kappers CU, Huber GC, Crosby EC (1967) The comparative anatomy of the nervous system of vertebrates, including man, vol III. Hafner Publishing Company, New York

Aziz TZ, Peggs D, Agarwal E, Sambrook MA, Crossman AR (1992) Subthalamic nucleotomy alleviates parkinsonism in the 1-methyl-4-phenyl-1,2,3,6-tetrahydropyridine (MPTP)-exposed primate. Br J Neurosurg 6(6):575–582

Bjarkam CR (2015) Neuroanatomi. 2. udgave. Munksgaard Danmark. ISBN 978-87-628-1206-2

Bjarkam CR, Pedersen M, Sørensen JC (2001) New strategies for embedding, orientation and sectioning of small brain specimens enable direct correlation to MR-images, brain atlases, or use of unbiased stereology. J Neurosci Methods 108:153–159

Bjarkam CR, Cancian G, Larsen M, Rosendahl F, Ettrup KS, Zeidler D, Blankholm AD, Østergaard L, Sunde N, Sørensen JC (2004) A MRI-compatible stereotaxic localizer box enables high-precision stereotaxic procedures in pigs. J Neurosci Methods 139(2):293–298

Bjarkam CR, Jorgensen RL, Jensen KN, Sunde NA, Sørensen JCH (2008a) Deep brain stimulation electrode anchoring using BioGlue®, a protective electrode covering, and a titanium microplate. J Neurosci Methods 168:151–155

Bjarkam CR, Nielsen MS, Glud AN, Rosendal F, Mogensen P, Bender D, Doudet D, Møller A, Sørensen JC (2008b) Neuromodulation in a minipig model of Parkinson disease. Br J Neurosurg 22(Suppl. 1):S9–S12

Bjarkam CR, Cancian G, Glud AN, Ettrup KS, Østergaard L, Sørensen JC (2009) Isocentric MRI-guided stereotaxic procedures in pigs based on a stereotaxic localizer box fitted with an adapted Leksell frame and use of related clinical computer-planning software. J Neurosci Methods 183(2):119–126

Bjarkam CR, Glud AN, Margolin L, Reinhart K, Franklin R, Deding D, Ettrup KS, Fitting LM, Nielsen MS, Sørensen JC, Cunningham MG (2010) Safety and function of a new clinical intracerebral microinjection instrument (IMI) for stem cells and therapeutics examined in the Göttingen minipig. Stereotact Funct Neurosurg 88(1):56–63

Bjarkam CR, Orlowski D, Tvilling L, Bech J, Glud AN, Sørensen JCH (2016) Exposure of the pig CNS for histological analysis; a manual to decapitation, skull opening and brain removal. J Vis Exp **(under review)**

Brodmann K (1909) Vergleichende Lokalisationslehre der Grosshirnrinde. J.A. Barth, Leipzig

Cajal SR (1904) Textura del sistema nervioso del hombre y de los vertebrados. Tomo II, segunda parte, Madrid [Translated by Pasik P and Pasik T, and presented as Cajal SR, Texture of the nervous system of man and the vertebrates, vol III. Springer, Wien (2002)]

Campbell AW (1905) Histological studies on the localisation of cerebral function. University Press, Cambridge

Chaillou E, Tillet Y (2005) Nutrition and hypothalamic neuropeptides in sheep: histochemical studies. Histol Histopathol 20(4):1209–1225

Craner SL, Ray RH (1991a) Somatosensory cortex of the neonatal pig: I. Topographic organization of the primary somatosensory cortex (SI). J Comp Neurol 306:24–38

Craner SL, Ray RH (1991b) Somatosensory cortex of the neonatal pig: II. Topographic organization of the secondary somatosensory cortex (SII). J Comp Neurol 306:39–48

Cumming P, Gillings NM, Jensen SB, Bjarkam CR, Gjedde A (2003) Kinetics of the uptake and distribution of the dopamine D2/3 agonist (*R*)-*N*-[1-11C]*n*-propylnorapomorphine in brain of healthy and MPTP-poisoned Gottingen miniature pigs. Nucl Med Biol 30(5):547–553

Dalmose A, Bjarkam CR, Sørensen JC, Jørgensen TM, Djurhuus JC (2004) Effects of high frequency deep brain stimulation on urine storage and voiding function in conscious minipigs. Neurourol Urodyn 23(3):265–272

Dalmose A, Bjarkam CR, Djurhuus JC (2005) Stereotactic electrical stimulation of the pontine micturition center in the pig. Br J Urol 95:886–889

Danielsen EH, Smith DF, Poulsen PH, Østergaard L, Gee A, Ishizu K, Venkatachalam TK, Bender D, Hansen S, Gjedde A, Scheel-

Krüger J, Møller A (1998) Positron emission tomography of living brain in minipigs and domestic pigs. Scand J Lab Anim Sci Suppl 25(1):127–135

Danielsen EH, Cumming P, Andersen F, Bender D, Brevig T, Falborg L, Gee A, Gillings NM, Hansen SB, Hermansen F, Johansen J, Johansen TE, Dahl-Jørgensen A, Jørgensen HA, Meyer M, Munk O, Pedersen EB, Poulsen PH, Rodell AB, Sakoh M, Simonsen CZ, Smith DF, Sørensen JC, Østergaard L, Zimmer J, Gjedde A, Møller A (2000) The DaNEX study of embryonic mesencephalic, dopaminergic tissue grafted to a minipig model of Parkinson's disease: Preliminary findings of effect of MPTP poisoning on striatal dopaminergic markers. Cell Transplant 9:247–259

Dinopoulos A, Karamanlidis AN, Papadopoulos G, Antonopoulos J, Michaloudi H (1985) Thalamic projections to motor, prefrontal and somatosensory cortex in sheep studied by means of the horseradish peroxidase retrograde transport method. J Comp Neurol 241:63–81

Dolezalova D, Hruska-Plochan M, Bjarkam CR, Sørensen JC, Cunningham MG, Weingarten D, Ciacci JD, Juhas S, Juhasova J, Motlik J, Hefferan MP, Hazel T, Johe K, Carromeu C, Muotri A, Bui J, Strnadel J, Marsala M (2014) Pig models of neurodegenerative disorders: utilization in cell replacement-based preclinical safety and efficacy studies. J Comp Neurol 522(12):2784–2801

Ettrup K, Sørensen JC, Bjarkam CR (2010) The anatomy of the Göttingen minipig hypothalamus. J Chem Neuroanat 39(3):151–165

Ettrup KS, Glud AN, Orlowski D, Fitting LM, Meier K, Soerensen JC, Bjarkam CR, Olsen Alstrup AAK (2011a) Basic surgical techniques in the Göttingen minipig: intubation, transurethral bladder catheterization, femoral vessel catheterization, and transcardial perfusion. J Vis Exp 52:2652

Ettrup KS, Tornøe J, Sørensen JC, Bjarkam CR (2011b) A surgical device for minimally invasive implantation of experimental deep brain stimulation leads in large research animals. J Neurosci Methods 200(1):41–46

Ettrup KS, Sørensen JC, Rodell A, Alstrup AKO, Bjarkam CR (2012) Hypothalamic deep brain stimulation influences autonomic and limbic circuitry involved in the regulation of aggression and cardiocerebrovascular control in the Göttingen minipig. Stereotact Funct Neurosurg 90(5):281–291

Fang M, Li J, Rudd JA, Wai SM, Yew JCC, Yew DT (2006) fMRI mapping of cortical centers following visual stimulation in postnatal pigs of different ages. Life Sci 78:1197–1201

Fast R, Rodell A, Gjedde A, Mouridsen K, Alstrup AK, Bjarkam CR, West MJ, Berendt M, Møller A (2013) PiB fails to map amyloid deposits in cerebral cortex of aged dogs with canine cognitive dysfunction. Front Aging Neurosci 5:99

Fèlix B, Lèger M-E, Albe-Fessard D, Marcilloux JC, Rampin O, Laplace JP (1999) Stereotaxic atlas of the pig brain. Brain Res Bull 49(1/2):1–138

Fjord-Larsen L, Kusk P, Tornøe J, Juliusson B, Torp M, Bjarkam CR, Nielsen MS, Aa Haandberg, Sørensen JC, Wahlberg LU (2010) Long-term delivery of nerve growth factor by encapsulated cell biodelivery in the Göttingen minipig basal forebrain. Mol Ther 18(12):2164–2172

Glud AN, Hedegaard C, Nielsen MS, Sørensen JC, Bendixen C, Jensen PH, Larsen K, Bjarkam CR (2010) Direct gene transfer in the Göttingen minipig CNS using stereotaxic lentiviral microinjections. Acta Neurobiol Exp 70:1–8

Glud AN, Hedegaard C, Nielsen MS, Sørensen JC, Bendixen C, Jensen PH, Mogensen PH, Larsen K, Bjarkam CR (2011) Direct MRI-guided stereotaxic viral mediated gene transfer of alpha-synuclein in the Göttingen minipig CNS. Acta Neurobiol Exp (Wars) 71(4):508–518

Hadziselimovic H, Dilberovic F (1977) Appearance of the wild boar brain. Acta Anat 98:14–20

Herec S (1967) Structure of the olfactory tubercle and nucleus of the diagonal tract of Broca in the pig. Folia Morph 26(4):452–458

Herre W (1936) Untersuchungen an hirnen von wild- und hausschweinen. Verhandlungen der Deutschen Zoologischen Gesellschaft, pp 200–211

Holm IE, Geneser FA (1989) Histochemical demonstration of zinc in the hippocampal region of the domestic pig: I. Entorhinal area, parasubiculum, and presubiculum. J Comp Neurol 287:145–163

Holm IE, Geneser FA (1991a) Histochemical demonstration of zinc in the hippocampal region of the domestic pig: II. Subiculum and hippocampus. J Comp Neurol 305:71–82

Holm IE, Geneser FA (1991b) Histochemical demonstration of zinc in the hippocampal region of the domestic pig: III. The dentate area. J Comp Neurol 308:409–417

Igarashi S, Kamiya T (1972) Atlas of the vertebrate brain. University of Tokyo Press, Tokyo

Jelsing J, Hay-Schmidt A, Dyrby T, Hemmingsen R, Uylings HBM, Pakkenberg B (2006a) The prefrontal cortex in the Göttingen minipig brain defined by neural projection criteria and cytoarchitecture. Brain Res Bull 70:322–336

Jelsing J, Nielsen R, Olsen AK, Grand N, Hemmingsen R, Pakkenberg B (2006b) The postnatal development of neocortical neurons and glial cells in the Göttingen minipig and the domestic pig brain. J Exp Biol 209:1454–1462

Jensen KN, Deding D, Sørensen JC, Bjarkam CR (2009) Long-term implantation of deep brain stimulation electrodes in the pontine micturition centre of the Göttingen minipig. Acta Neurochir 151(7):785–794

Kruska D (1970) Vergleichend cytoarchitektonische untersuchungen an gehirnen von wild- und Hausschweinen. Z Anat Entwickl Gesch 131:291–324

Kruska D (1972) Volumenvergleich optischer hirnzentren bei wild- und hausschweinen. Z Anat Entwickl Gesch 138:265–282

Kruska D, Stephan H (1973) Volumenvergleich allokortikaler hirnzentren bei wild- und hausschweinen. Acta Anat 84:387–415

Kyllar M, Stembirik J, Putnová I, Stehlik L, Odehnalová S, Buchtová M (2014) Radiography, computed tomography and magnetic resonance imaging of craniofacial structures in pig. Anat Histol Embryol 43(6):435–452

Larsen M, Bjarkam CR, Stoltenberg M, Sørensen JC, Danscher G (2003) An autometallographic technique for myelin staining in formaldehyde-fixed tissue. Histol Histopathol 18(4):1125–1130

Larsen M, Bjarkam CR, Østergaard K, West MJ, Sørensen JC (2004) The anatomy of the porcine subthalamic nucleus evaluated with immunohistochemistry and design based stereology. Anat Embryol 208(3):239–247

Lind MN, Moustgaard A, Jelsing J, Vajta G, Cumming P, Hansen AK (2007) The use of pigs in neuroscience: modeling brain disorders. Neurosci Biobehav Rev 31:728–751

Lunau H (1956) Vergleichend-metrische untersuchungen am allocortex von wild- und hausschweinen. Zeitschrift für Mikroskopisch-Anatomische Forschung 62:673–698

Mikkelsen M, Moller A, Jensen LH, Pedersen A, Harajehi JB, Pakkenberg H (1999) MPTP-induced Parkinsonism in minipigs: a behavioral, biochemical, and histological study. Neurotoxicol Teratol 21:169–175

Nielsen MS, Sørensen JC, Bjarkam CR (2009) The substantia nigra pars compacta of the Göttingen minipig: an anatomical and stereological study. Brain Struct Funct 213(4–5):481–488

Nielsen MS, Glud AN, Møller A, Mogensen P, Bender D, Sørensen JC, Doudet D, Bjarkam CR (2016) Continuous MPTP intoxication in the Göttingen minipig results in chronic parkinsonian deficits. Acta Neurobiol Exp 76:198–210

Palmieri G, Farina V, Panu R, Asole A, Sanna L, De Riu PL, Gabbi C (1987) Course and termination of the pyramidal tract in the pig. Arch Anat Microsc 75(3):167–176

Paxinos G, Watson C (2007) The rat brain in stereotaxic coordinates, 6th edn. Academic Press, New York

Plogmann D, Kruska D (1990) Volumetric comparison of auditory structures in the brains of european wild boars (*Sus scrofa*) and domestic pigs (*Sus scrofa* f. dom.). Brain Behav Evol 35:146–155

Røhl L, Sakoh M, Simonsen CZ, Vestergaard-Poulsen P, Sangill R, Sørensen JC, Bjarkam CR, Stødkilde-Jørgensen H, Gyldensted C, Østergaard L (2002) Time evolution of cerebral perfusion and ADC measured by MRI in a porcine stroke model. J Magn Reson Imaging 15(2):123–129

Rose JE (1942) A cytoarchitectural study of the sheep cortex. J Comp Neurol 76(1):1–55

Rosendal F, Bjarkam CR, Larsen M, Hansen HE, Madsen M, Sørensen JC, Mortensen J (2005) Does chronic low dose treatment with ciclosporin influence the brain? A histopathological study in pigs. Transplant Proc 37(8):3305–3308

Saikali S, Meurice P, Sauleau P, Eliat P-A, Bellaud P, Randuineau G, Vérin M, Malbert C-H (2010) A three-dimensional digital segmented and deformable brain atlas of the domestic pig. J Neurosci Methods 192:102–109

Salinas-Zeballos M-E, Zeballos GA, Gootman PM (1986) A stereotaxic atlas of the developing swine (*Sus scrofa*) forebrain. In: Tumbleson ME (ed) Swine in biomedical research. Plenum Press, New York, pp 887–906

Sauleau P, Lapouble E, Val-Laillet D, Malbert CH (2009) The pig model in brain imaging and neurosurgery. Animal 3(8):1138–1151

Sisson S, Grossman JD (1956) The anatomy of the domestic animals, 4th edn. W. B. Saunders Company, Philadelphia

Solnitzky O (1938) The thalamic nuclei of *Sus scrofa*. J Comp Neurol 69:121–169

Sørensen JC, Bjarkam CR, Simonsen CZ, Danielsen E, Geneser FA (2000) Oriented sectioning of irregular tissue blocks in relation to computerized scanning modalities. Results from the domestic pig brain. J Neurosci Methods 104:93–98

Sørensen JC, Nielsen MS, Rosendal F, Deding D, Ettrup KS, Jensen KN, Jørgensen RL, Glud AN, Meier K, Fitting LM, Møller A, Alstrup AK, Ostergaard L, Bjarkam CR (2011) Development of neuromodulation treatments in a large animal model—do neurosurgeons dream of electric pigs? Prog Brain Res 194:97–103

Stephan H (1951) Vergleichende untersuchungen über den feinbau des hirnes von wild- und haustieren. Zoologisches Jahrbuch, Abteilung für Anatomie und Ontogenie 71:487–586

Szteyn S, Galert D, Dynowski J, Hoczyk W (1980) The stereotaxic configuration of hypothalamus nerve centers in the pig. Anatomischer Anzeiger 147:12–32

Watanabe H, Andersen F, Simonsen CZ, Evans SM, Gjedde A, Cumming P, The DaNex Study Group (2001) MR-based statistical atlas of the Göttingen minipig brain. Neuroimage 14:1089–1096

Woolsey CN, Fairman DF (1946) Contralateral, ipsilateral, and bilateral representation of cutaneous receptors in somatic areas I and II of the cerebral cortex of pig, sheep, and other mammals. Surgery 19:684–702

Yoshikawa T (1968) The brain of the pig (Yorkshire breed). In: Atlas of the brains of domestic animals. University of Tokyo Press, Tokyo